Automatic detection of the HFO zone in epilepsy using magnetoencephalography.

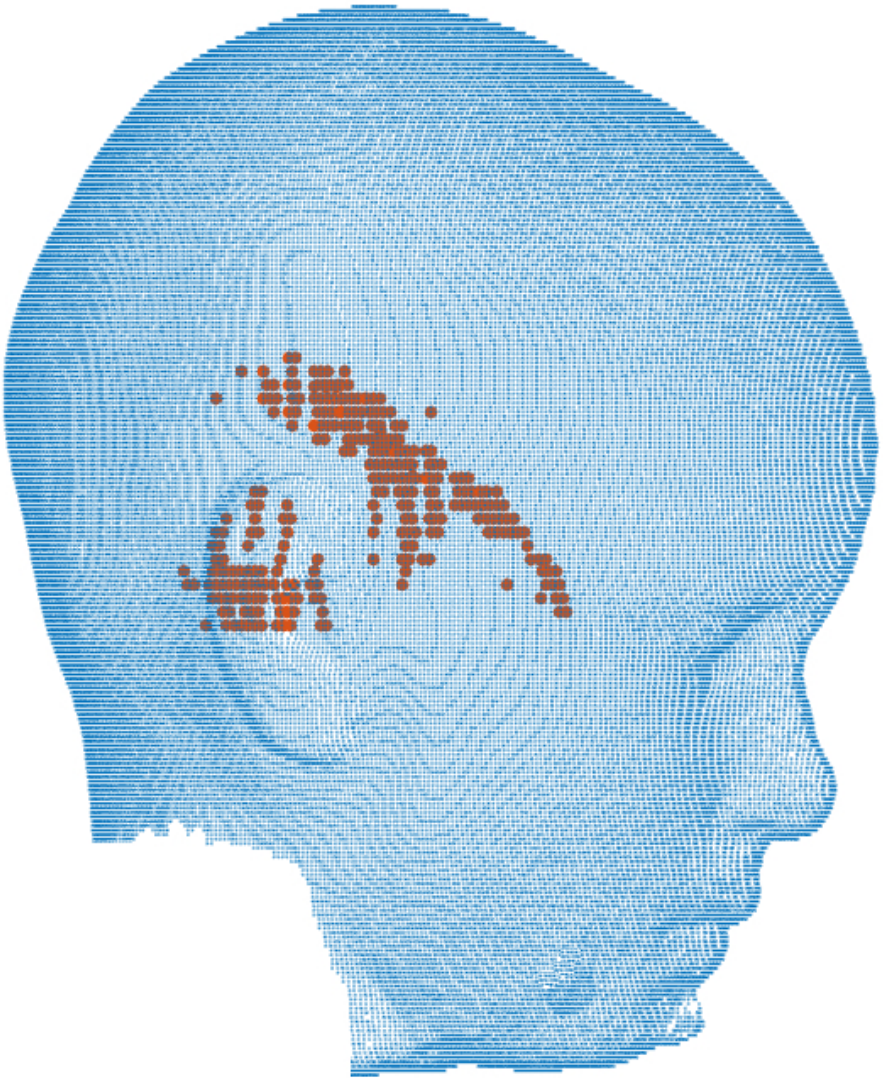

Frank van Rosmalen
Faculty of Science and Technology
University of Twente
November 2015

UNIVERSITY OF TWENTE. UMC Utrecht VUmc

Master thesis:
Automatic detection of the HFO zone in epilepsy using magnetoencephalography, november 2015
Frank van Rosmalen

Graduation Committee:
Prof. dr. ir. M.J.A.M. van Putten [a] (Chairman, Technical Supervisor)
Dr. G.J.M. Zijlmans [b,c,d] (Medical Supervisor)
Dr. ir. A. Hillebrand [c] (Technical Supervisor)
N.E.C. van Klink, MSc [b] (Daily Supervisor)
Drs. P.A. van Katwijk [e] (Mentor)
Dr. ir. B. ten Haken [f] (External Supervisor)

Institution:
[a] Department of Clinical Neurophysiology, Universiteit Twente
[b] Brain Center Rudolf Magnus, department of Neurology and Neurosurgery, UMC Utrecht
[c] Department of Clinical Neurophysiology and Magnetoencephalography Center, VU Medical Center
[d] SEIN – Stichting Epilepsy Instellingen Nederland
[e] Twente University
[f] Department of NeuroImaging, Twente University

Contents

1 Acronyms and parameters

Acronyms

AED	Anti-epileptic drug
cxSSS	Covariance-based (c) and uncorrelated noise subtracted by cross-validation (x) extension of SSS
EEG	Electroencephalography
ECoG	Electrocorticogram
EOI	Event of interest
EZ	Epileptogenic zone
FDG	Fludeoxyglucose
HFO	High frequency oscillation
HiFP	High frequency peak
iEEG	intracranial EEG
IRR	Infinite impulse response
LoFP	Low frequency peak
MEG	Magnetoencephalography
MRI	Magnetic resonance imaging
PET	Positron emission tomography
RMS	Root mean square
SD	Standard deviation
SNR	Signal-to-noise ratio
SOZ	Seizure onset zone
SPECT	Single positron emission computed tomography
SSS	Signal space separation
tSSS	Temporal extension of SSS
VS	Virtual sensor

Parameters

BW	Bandwidth used for the calculation of the beamformer weights.
$BLmu$	Indicating the percentage of the maximum entropy which should be exceeded for a sample to classify as baseline in the HFO detector.
$BLst\_freq$	The lowest frequency where the detector algorithm should look for baseline.
$bound\_min\_peak$	Lower boundary for the high frequency peak in the HFO detector.
C	The covariance matrix used to calculate the beamformer weights.
$CDFlevel$	Determines where the cut-off value for the cumulative density function of the HFO detector is placed.
ΔC	The difference between an analytically derived and measured covariance matrix.
dur	Indicates how many seconds the HFO detector has to search for baseline samples before continuing to the next step.
$maxIntervalToJoin$	The minimum interval between detected EOIs in the HFO detector, otherwise EOIs are merged.
$min\_HFO\_duration$	Minimum continuous length for HFOs found by the HFO detector.
min_trough	Minimum ratio between the high frequency peak and the through in the HFO detector.

2 Summary

Introduction Epilepsy is one of the most common diseases encountered by neurologists. Treatment with anti-epileptic drugs fails to sufficiently control seizure activity in 30% of epilepsy patients. When these patients suffer from a focal form of epilepsy, surgical removal of the epileptic focus can be considered. Current techniques to find this focus, called the epileptogenic zone (EZ) are either invasive, have a low spatial resolution or are unable to measure the relevant electrophysiological signals. This study combined the high spatial resolution of magnetoencephalography (MEG) with an automatic detector for an electrophysiological biomarker, high frequency oscillations (HFOs), to propose a hypothesis for the location of the EZ. HFOs are oscillations in the 80-500 Hz range, occurring in the EZ. It was shown very recently that HFOs can be visualised in MEG recordings using a spatial filtering technique called beamforming. Beamforming is used to reconstruct signals coming from a specific location in the brain. The signal created by the beamformer is called a virtual sensor (VS). This technique applies a weighing factor to the MEG signal to exclude noise from sources distant from the area of interest, thereby increasing signal-to-noise ratio (SNR) of the signal. The goal of this thesis was to increase the SNR of the signal to allow the use of an automatic detector to locate HFOs. When the optimal combination of pre-processing and beamforming techniques are found, VSs are calculated covering the total brain. Automatically detected HFOs in these VSs should point towards the EZ.

Methods A retrospective dataset consisting of the resting state MEG data of 8 patients with epilepsy was used. A total of 70 VSs were calculated for each patient, divided in 2 star shapes. One star was placed with the center in the epileptic spiking activity (that was marked for a previous study on the same dataset), the other on the contralateral side of the brain to function as control. The location of the HFOs was known for all VSs in all patients (also from the previous study on this dataset). First the SNR was optimized by changing the settings of the beamformer by changing the length (T_{cov}) and the bandwidth (BW) of the signal used to calculate the beamformer weights. Three pairs of settings were chosen: 1) T_{cov}: a 200 ms window around marked spikes, BW: 80-500 Hz. 2) T_{cov}: full recording length, BW: 80-500 Hz. 3) T_{cov}: full recording length, BW 80-250 Hz. Differences in the constructed VSs signals were quantified by calculating the SNR per VS per patient. The SNR was calculated as the average power in the 80-500 Hz band in the parts marked as HFO, divided by the average power in the same band for the parts not marked as HFO.

After determining the best settings for the beamformer, two spatial filtering pre-processing steps were compared. The commonly used temporal extension of the signal space separation (tSSS) method was compared to an extension of tSSS called cxSSS (which stands for covariance-based (c) and uncorrelated noise subtracted by cross-validation (x) SSS) which is currently in development. The comparison was based on the SNR of the signals, calculated as described above. This comparison was done for one patient due to technical difficulties.

The best beamformer settings and the best spatial filtering technique were used to calculate VSs on the 70 locations mentioned earlier. These VSs were used to optimize the HFO detector created by Burnos *et al.*. Optimization consisted of changing detection parameters and adding custom code to improve the detection of HFOs in MEG data. The main goal for the optimization was the reduction of false positive detections.

The last step in this thesis was the application of the best beamformer settings, the best spatial filtering technique and the optimized HFO detector to the total brain volume of one patient. VSs were calculated for approximately 24.000 locations evenly spread throughout the brain, and the HFO detector was applied to all VSs. The result was compared to the information from the (pre-)surgical evaluation.

Results No significant difference could be found between the three different beamformer settings, but visual inspection showed a reduction in noise for pair 2, where the full recording and the 80-500 Hz bandwidth were used for calculation of the beamformer weight. Since this method reduces noise and does not need a human reviewer, this method was chosen as best method.

The comparison of the two pre-processing techniques showed a significant difference, where the cxSSS method produced a higher SNR in comparison to the tSSS algorithm, although this could only be tested for one patient. It was chosen to use the cxSSS data for this patient for the rest of the analysis in this thesis.

Optimization of the HFO detector reduced the number of false positives from 86 to 13 moments in time,

but also reduced the number of true positives from 21 to 16. This was considered reasonable, since only moments showing a few HFOs were lost for the detection, and the moments where multiple channels showed HFOs at the same time were still correctly marked as HFO.

Application of the HFO detector to the total brain yielded a localization of the possible EZ to the correct side of the brain, but showed a very spread area where HFOs were detected. A better localization was shown when only the HFOs for a single moment in time were considered. The result of this analysis was in concordance with information from the pre-surgical evaluation and showed HFOs in the right temporo-occipital region. Electrophysiological investigation during surgery with electrodes directly on the brain showed that detected HFOs were spreading from a very small source located in the right occipital lobe of the patient.

Conclusion and discussion This study was the first to combine novel MEG techniques with an automatic HFO detector to localize the epileptogenic zone based on HFOs. It was possible to visualize HFOs in MEG using beamforming and to increase the SNR of the HFOs by using a combination of cxSSS pre-processing and beamformer settings. The SNR of the signal was successfully increased by using a new pre-processing algorithm and calculating the beamformer weights over the total length of the recording. By applying this knowledge to create VSs in the whole brain with a high SNR, the HFO detector was able to localize HFOs in the right temporo-occipital region.

Only one patient could be used for the final steps of the analysis, but more patients will be investigated in the near future. This will provide more information on the validity of the conclusions that the results in this thesis can be seen as a firm step towards a non-invasive, user independent technique that can be used to assist in the planning of epilepsy surgery.

3 Introduction

3.1 Clinical background

With a prevalence of 4.5-5.0 cases per 1000 people in Europe, epilepsy is one of the most common diseases encountered by neurologists [13]. The term epilepsy is used for multiple syndromes whose main feature is a predisposition to recurrent unprovoked seizures. Epilepsy can be categorized in generalized epilepsy; originating from alterations in either neuronal networks or intrinsic neuronal function, and focal epilepsy; either originating from a single location, or originating from multiple locations, called multifocal epilepsy [9]. The primary treatment of epilepsy is giving antiepileptic drugs (AEDs), but this treatment fails to sufficiently control seizure activity in 30% of the patients [29].

Epilepsy surgery is considered in patients with focal epilepsy who do not respond to AEDs. Accurate identification of the epileptic brain area is necessary to determine if the epilepsy has a focal origin and if so, to perform a resection. The epileptogenic zone (EZ) is a theoretical zone defined as the minimum amount of cortical tissue that must be resected to achieve seizure-freedom. This zone can be approximated by several biomarkers (figure 1), for example the seizure onset zone (SOZ) [24] which is the area of the cortex that initiates clinical seizures.

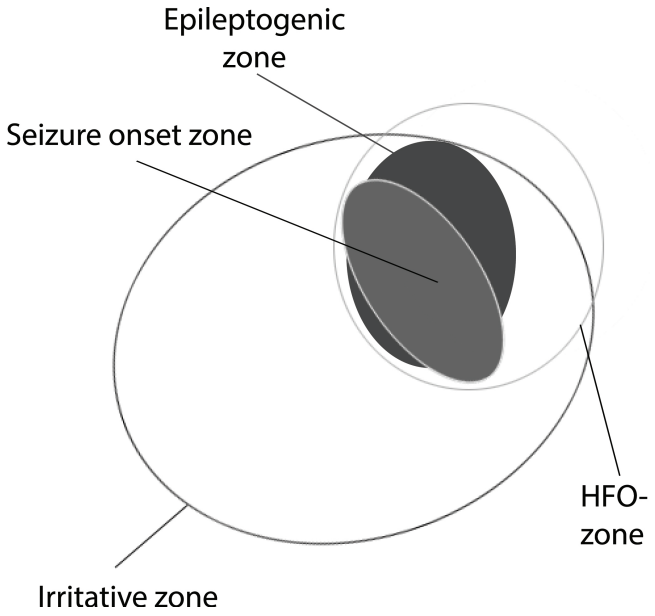

Figure 1: Different zones that can be used to estimate the epileptogenic zone in focal epilepsy. The seizure onset zone, where clinical seizures originate, the irritative zone, which generates interictal spikes and sharp waves and the HFO zone, which generates HFOs, are shown. The irritative zone is more widespread than the HFO zone, and the HFO zone has a better overlap with the epileptogenic zone [19].

Multiple techniques are used to estimate the location of the EZ. Video electroencephalography (EEG) monitoring determines the SOZ based on a combination of EEG changes and seizure semiology at the start and during of a seizure, where interictal EEG and magnetoencephalography (MEG) determine the EZ based on electrical and magnetic signals produced by the brain when there is no seizure present. Magnetic resonance imaging (MRI) is used to find lesions, which are often related to epilepsy. Other ways to estimate the EZ include positron emission tomography (PET) and ictal single-photon emission computed tomography (SPECT). When these non-invasive tests point to a clear epileptic focus, the patient is eligible for epilepsy surgery.

There is a balance between removing too much of the cortex, leading to a disruption of normal brain function, and removing not enough cortex tissue leading to incomplete seizure control [31]. Therefore invasive methods are used to form a hypothesis on the location of the epileptogenic zone. Grid or depth electrodes can be placed on and in the brain tissue, at locations based on the non-invasive pre-surgical tests, to determine which

tissue has to be resected. The neurophysiologist specifically looks for (inter)ictal epileptiform discharges to form a hypothesis on the epileptogenic zone. The most frequent form of epileptiform discharges is visible as spikes in the EEG and the area producing spikes is called the irritative zone.

Based on the methods mentioned, the success rate of epilepsy surgery is around 65%; in resections for temporal lobe epilepsy (TLE) 60- 90% of patients achieve seizure freedom while in extra-temporal epilepsy this is around 40-65% [45, 37]. The main reason for surgical failure is incomplete resection of the epileptogenic zone [15].

Resection of brain tissue producing spikes is under debate, because not all spikes may signify underlying epileptiform tissue as spikes may spread to surrounding healthy tissue, leading to an unnecessary large resection [2, 46]. A more specific biomarker for the epileptogenic zone could lead to an improvement of surgical outcome. High frequency oscillations (HFOs) have been proposed as a more specific biomarker for the epileptogenic zone.

3.2 High Frequency Oscillations (HFOs)

HFOs are short lasting oscillations with a frequency higher than 80 Hz and can be subdivided in ripples (80-250 Hz) and fast ripples (250-500 Hz). They are visible in the (intracranial-)EEG (after applying a high pass filter) and are defined as events with at least four consecutive oscillations that clearly rise above baseline [53] (figure 2). There are multiple theories about the origin of HFOs, but their cellular correlates are currently unknown. One of the theories states that pathological HFOs originate from out-of-phase firing of small groups of pathologically interconnected principal cells [12]. Morphological, molecular, and functional changes in epileptic tissue cause neurons to respond abnormally to sub-threshold stimuli or become spontaneously active. Firing of a single neuron, or a small neuronal population, may result in a fast recruitment of interconnected cells, resulting in synchronous action potential firing, which can be detected as an HFO [21].

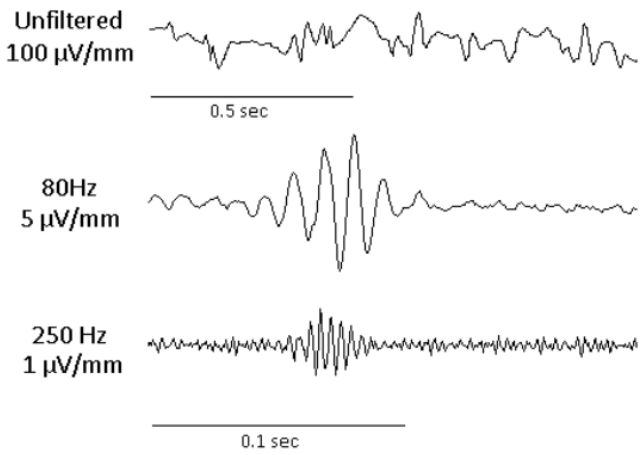

Figure 2: Example of an HFO found during intracranial EEG recording. The top trace is the unfiltered signal, the middle trace is the same signal, with an 80 Hz high pass filter and enlarged in time and amplitude. This oscillation is a ripple (80-250 Hz). The bottom trace shows the same signal as the middle trace, with a 250 Hz high pass filter. This oscillation is a fast ripple (250-500 Hz).

The first studies that investigated HFOs in humans were published in 1999 [6, 5], and multiple studies have confirmed the link between HFOs and the SOZ since [54, 20]. HFOs and spikes often occur together [39], but HFOs, with or without spikes, localized the SOZ more accurately than spikes alone [19]. It seems that HFOs are more related to epileptic activity than spikes, as rates of spikes increased after seizures while rates of HFOs and spikes with HFOs stayed the same [53, 52]. HFOs increase in rate from interictal to pre-ictal to ictal episodes, whereas spikes only increase from interictal to ictal, without a pre-ictal increase [52]. Another important finding of this latter study is that spikes were recorded on different electrodes during interictal

episodes compared to ictal episodes, while HFOs were detected on the same electrodes during all measured episodes. Retrospective studies on surgical outcome based on HFOs show that removal of tissue generating interictal HFOs correlates well with seizure freedom [41, 19, 48].

The gold standard for detecting HFOs in intracranial EEG is visual scoring. In a suitable EEG review program the screen is split in two windows, showing the signal with an 80 Hz high pass filter in one window, and the same signal with a 250 Hz high pass filter in the other. With a time scale of 0.8 s/page and the amplitude scale at 1.5 μV/mm, events showing an oscillation with at least four peaks clearly deviating from the baseline are marked as HFO. This is a time consuming process which may take up to one hour for a one-minute 10-channel signal [50].

Most research on HFOs is based on intracranial recordings, because the low signal-to-noise ratio (SNR) of non-invasive EEG makes it difficult to visually identify HFOs. Although some studies have shown that the measurement of HFOs in scalp EEG is possible [3, 25], an obstacle for scalp EEG measurements is the low spatial resolution caused by the use of relatively few electrodes in the standard 10-20 system. The wide spreading of the signal from the source to the EEG electrodes on the scalp is another downside of EEG. [18]. Non-invasive measurement of HFOs is less cumbersome for the patient and yields no side effects compared to invasive measurements. A technique that might overcome the obstacles of non-invasive HFO measurement using EEG is magnetoencephalography (MEG).

3.3 Magnetoencephalography (MEG)

MEG records magnetic fields generated by neuronal sources in the brain. These magnetic fields are produced by the same electrical signals that are measured with EEG. The advantage of measuring magnetic fields instead of electrical signals is that magnetic signals are not (or very little) disturbed by the scalp and other tissue covering the brain [14]. MEG can achieve a high spatial resolution because there is no spreading of the signals caused by volume conduction, as is the case in EEG [14], and because it uses more sensors compared to standard 10-20 EEG.

The first suggestion that HFOs could be found in MEG was based on the analysis of artificially generated MEG data [27]. Around the same time, the first study showed HFOs in real MEG signals based on frequency analysis by using accumulated spectrograms, where a good correlation between HFOs and the SOZ was found in nine out of twelve patients [49]. Another study recorded intracranial EEG and MEG simultaneous, and used automatically detected intracranial HFOs as a trigger for channel-specific averaging of the MEG signal. HFOs were not visible in the non-averaged MEG traces, but were detectable in averaged spectrograms of the same signal. The reconstructed HFO source location was concordant with the SOZ in five out of six patients [28]. Ictal HFOs in MEG were also investigated using combined EEG/MEG measurements in patients with childhood absence epilepsy. Time-frequency plots of the MEG signal during a seizure revealed high frequency activity, and source localization showed that HFOs provide extra information about activated brain regions during absence seizures [38]. Another study that investigated HFOs in childhood absence epilepsy using spectrograms concluded that HFOs tend to spread less compared to spikes [26], in line with invasive studies [52].

All of the MEG studies mentioned above used (averaged) spectrograms to quantify HFOs and did not identify individual HFOs in the time domain, as is typically done in intracranial EEG. Therefore it is difficult to determine if the high frequency activity identified in the spectra is the same as the time domain HFOs. Visual identification of HFOs in MEG in the time domain proves to be challenging. One of the main reasons for this is the high level of noise, caused by the environment (e.g. power lines producing a 50 Hz signal), by the MEG setup itself (e.g. the head localization coils producing a 300 Hz signal), or caused by the patient (e.g. movement- or muscle- artifacts). Because of this noise it is difficult to distinguish HFOs from the background.

A recently published study was the first to identify HFOs in the time domain in MEG data [40]. The author showed that HFOs could be visually identified in 8 out of 12 patients after applying spatio-temporal signal space separation (tSSS) and a spatial filtering technique called beamforming (see below). Beamforming can be used to calculate so-called 'virtual sensors' (VSs), time traces that show the activity at fixed locations in the brain.

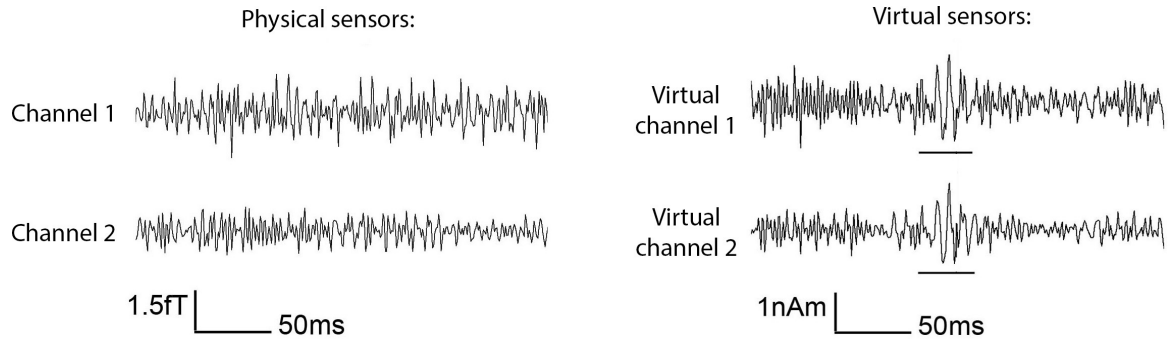

Figure 3: MEG physical sensor channels (left) and virtual sensor channels (right) of the same epoch of the same brain region for two channels, filtered with an 80 Hz high pass filter. Beamformer analysis revealed an HFO (underlined) that is not visually detectable in the physical sensors over the same region of the brain.

Van Klink et al. showed an increase in SNR by placing 35 VSs in the brain in a 3-dimensional star shaped configuration with an inter-VS distance of 1 cm. The core of the star was placed in the irritative zone, based on the already marked spikes in the physical sensors channels. An identical configuration of 35 VSs was placed on the contralateral side to serve as control, leading to 70 VSs in total. For each of the 12 patients, 10 minutes of resting state data was analyzed. Beamformer analysis made it possible to visualize HFOs that were not visible in the physical sensors (figure 3).

Van Klink ıet al. used only 35 VSs in each hemisphere because of the amount of time it takes to review the channels, as was described earlier. This forms a restriction to the applicability of beamformer analysis. Ideally VSs would be placed in the entire brain to be sure not to miss HFOs due to spatial under-sampling. Automatic detection of HFOs in MEG would speed up the analysis and enable sampling of the whole brain, which would enable the generation of a 'heat-map' for HFOs, showing regions with a high HFO count in the brain.

Localizing the epileptogenic zone based on HFOs in MEG is a technique in development. It was shown that it is possible to increase the SNR of MEG by using a beamformer algorithm to create virtual sensors [40]. This was the first time that HFOs were visually identifiable in MEG recordings in the time domain. The downside of visual detecting HFOs is that it takes a long time to analyze the data, which is a practical limitation for the amount of VSs placed in the brain. This might lead to spatial under sampling of the brain and thus missing important information for the hypothesis of the location of the epileptogenic zone. To avoid under sampling, VSs should ideally cover the whole brain to find HFOs. This process is not straightforward because of the large amount of data acquired.

The signal quality can be improved by using the optimal settings for the beamformer algorithm. This should lead to a reduction of noise and thus a higher SNR. The large amount of data can be analyzed by an automatic HFO detector optimized for MEG data. This requires an algorithm that is fast enough to be used for clinical purposes.

3.4 Research questions and thesis outline

The question to be answered in this report is: is it possible to automatically locate the HFO zone based on virtual MEG sensors? The following steps are used to answer this question:

1. Optimization of the MEG signal processing. A high SNR is necessary to be able to discern HFOs in the MEG signals, so the first steps are aimed at improving the signal quality.
    (a) Find optimal beamformer settings. The paper by van Klink *et al.* used a standard beamformer algorithm to show that it is possible to visualize HFOs in MEG. Optimization of the settings of the beamformer can increase the SNR of the VSs signals. The results of the optimized beamformer will be compared with the beamformer results from the article by van Klink *et al.*

(b) Compare different pre-processing techniques in combination with the optimal beamformer settings to increase the SNR of the signal.

2. Detection of HFOs and application to VSs.

   (a) Search for an automatic detection algorithm that can detect HFOs in MEG.

   (b) Optimize the best detector for MEG data.

3. Application to patient data.

   (a) Calculate VSs for the whole brain and apply the detector to all acquired signals.

   (b) Use the number of detected HFOs to predict the location of the epileptogenic zone, by comparison with the known irritative zone, seizure onset zone, visually scored HFO zone and if possible the pre-surgical workup and surgical resection.

Chapter two discusses the patient population and the acquisition of the data used for this study. Chapter three describes the optimization of the MEG signal by using spatio-temporal signal space separation and different settings for a beamformer algorithm. In chapter four a short review of recent automatic HFO detectors is given, and the automatic HFO detector used in the report is introduced. Chapter five shows the results of the application of the HFO detector in the total brain volume. Chapter six gives the conclusion and points of discussion for this project. The last chapter, chapter seven, covers some of the future perspectives on the automatic detection of the HFO zone using MEG.

A preliminary version of the results of this thesis were presented at the International Epilepsy Conference in September 2015 in Istanbul. The abstract and the poster presented at the conference are included in Appendix A and B.

4 Patients

This study uses retrospective MEG data, which is the same dataset as used in by van Klink *et al.* [40], consisting of 12 patients with refractory epilepsy who underwent MEG registration at the VU University Medical Center Amsterdam in 2013. Patients underwent MEG registration to improve the delineation of an unclear EEG-focus. Patients without epileptic spikes in the MEG recording were excluded, since the study by van Klink *et al.* used spikes to determine the locations of the VSs (see below). All patients or their caretakers gave written informed consent prior to the clinical MEG recording.

The recordings were made when the patients had their eyes closed and no task was given. Each recording was approximately 15 minutes. Patients were recorded in supine position in order to minimize head movements. MEG data was recorded with a 306-channel whole-head Elekta system (Elekta Neuromag Oy, Helsinki, Finland) in a magnetically shielded room (VacuumSchmelze GmbH, Hanau, Germany). The MEG system consists of 102 sensor units, and each unit contains two orthogonal planar gradiometers and one magnetometer. Four or five head-localization coils were used to continuously record the position of the head relative to the MEG sensors. The data were recorded using a sample frequency of 1250 Hz, an anti-aliasing filter of 410 Hz and a high pass filter of 0.1 Hz. The raw data were spatially filtered using the temporal extension of signal space separation (tSSS) applied with MaxFilter software (Elekta Neuromag Oy, version 2.1) [36, 34]. This pre-processing step is explained in more detail in the next chapter. Epileptic spikes in the recording were marked manually for each patient. After marking of the spikes VSs were calculated for 70 locations in the brain. The 70 VSs were divided in two pairs of 35 VSs each, both arranged in a star shape. The center of one star was placed at the center of the epileptic spikes, the other star was placed on the contralateral side of the brain to function as control (see figure 4). Patient details are summarized in table 1.

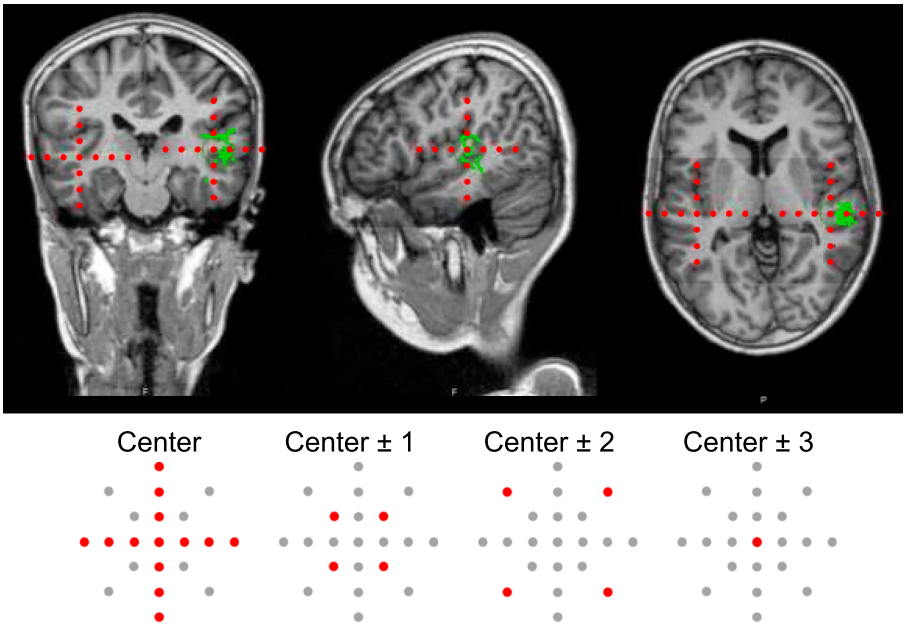

Figure 4: Example of the virtual sensor placement for patient 9. The 70 virtual sensors are divided in 2 star shapes. One star is placed with the center of the star in the focus of the epileptic spikes, the other on the contralateral side of the head to function as control. Figure adapted from [40].

A T1-weighted structural Magnetic Resonance Image (MRI) of each patient was made before the MEG measurement. The positions of the head-localization coils in the MEG and the outline of the patients scalp were digitized and custom surface matching software was subsequently used to co-register the MRI and MEG data. A single sphere fitted to the outline of the scalp was used as volume conductor model. This model was used with all analysis described in this thesis.

Part of the results in this paper are based on the data of one patient, patient 9. This patient is a 15 year

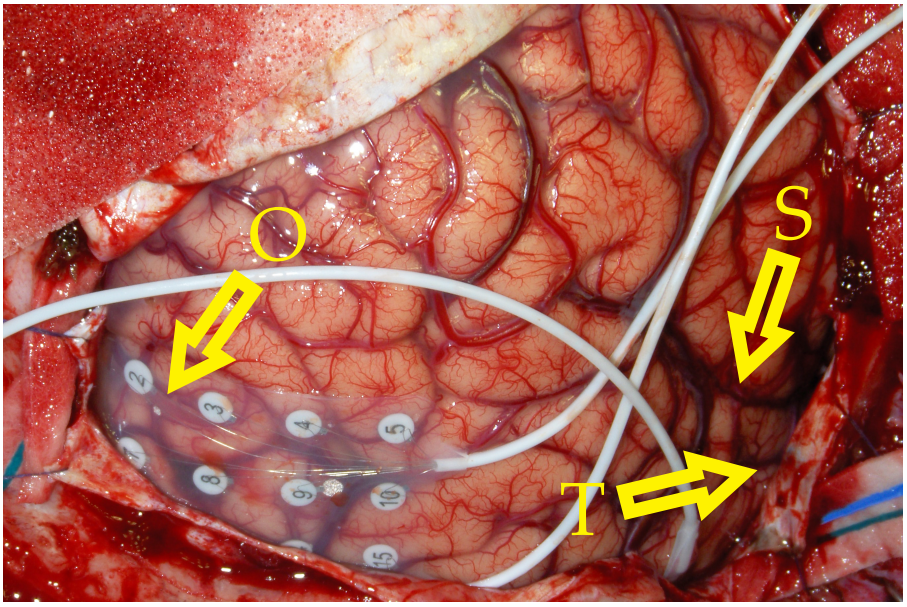

Figure 5: Placement of ECoG electrodes for patient 9. The electrode grid that is shown on the bottom left side consists of 4 x 5 electrodes with a contact surface 4.2 mm^2 per electrode. This grid can be placed directly on the brain for a high quality signal. Using this method a small occipital focus was discovered in patient 9. O: occipital lobe, S: lateral sulcus, T: temporal lobe.

old man suffering from refractory epilepsy after a pneumococcal meningitis. Seizure semiology is as follows: the patient feels 'weak' in the head, looks for a family member or school teacher. The patient folds his hands and is quiet. If this is the end of the seizure, the patient calls it a small seizure. If not, the patient starts staring with his eye wide open and makes swallowing sounds accompanied by bimanual and bipedal automatisms and ictal vocalizations. Duration of the seizure is one to one and a half minutes. The patient sometimes complains about headaches after a seizure. The small seizures occur 10-15 times each day. The longer seizures occur approximately 3 times per month.

MRI showed a right occipital gliosis. This is confirmed by FDG-PET, which also showed a reduced uptake right parietal and temporal, and in the right hippocampus. Result of the MEG source localization based on sharp waves, spike-wave complexes and spikes showed a lateralization to the right hemisphere, most likely neocortical posterior temporal, but an extratemporal origin could not be ruled out. SPECT showed a hyperperfusion right temporal-parietal over a large area. EEG showed a continuous irregular rhythm over the left fronto-temporal region and epileptiform discharges over the right hemisphere, mostly temporal.

The hypotheses after imaging and electrographic investigation was a parieto-temporal-occipital seizure onset, spreading to mesio-temporal structures for the elementary seizures, and to mesial, lateral temporal, orbitofrontal and mesiofrontal during complex seizures. This hypothesis was investigated using depth electrodes. A total of 12 depth electrodes were implanted, 10 in the right parieto-temporal-occipital region based on PET, SPECT, EEG and MEG, and 2 in the left temporofrontal region based on EEG. The depth electrodes picked up multiple seizures, but it was not able to localize a potential epileptogenic zone.

It was decided to continue investigating using electro-corticograpy (ECoG). This is done intra-operative by placing a grid of electrodes directly on the brain (see figure 5). The yield of the ECoG was epileptic activity in a small focus on the right occipital lobe, matching with the gliosis revealed by the MRI, and epileptic activity in the right hippocampus. The information from the ECoG combined with the depth EEG lead to the hypothesis that the activity found by imaging and scalp EEG was the result of spreading epileptiform activity that originated from the small occipital focus which was removed during surgery. Pathology showed gliosis in the parieto-occipital leasion and mesiotemporal sclerosis (Wyler grade IV, ILAE grade 1) in the hippocampus. At the moment of writing, the patient has been seizure free for 2 months.

Pt. nr.	Gender/ age	Affected MEG side	MRI findings	Interictal EEG abnormalities	Ictal EEG onset	PET	SPECT	Pathology	Surgery	HFOs
2	M/15	R/Temporal	Multiple cortical tubers, decreased grey and white matter differentiation R temporal	R fronto-tempero-basal	R, not localizing	-	R temporal	Tuber, no MTS	R neocortico-amygdalahippocampectomy, seizure free 3 months	7 (41)
3	M/16	R/Temporal	-	R anterior temporal	R temporal	R temporal	R temporal	Normal tissue	R temporo-lobectomy with amygdalahippocampectomy, seizure free 2 months	14 (4)
4	F/16	L/Parietal	Minimal white matter malformation R frontal	L abnormalities	R or L in different seizures.	No abnormalities	L temporal	No surgery	No surgery	2 (1)
5	F/17	R/Parietal	-	Fronto-central midline, probably more L	Fronto-central	R central	-	No surgery	No surgery	6 (1)
6	M/10	L/Frontal	Arachnoidal cyst L temporal	Bilateral frontal and generalized	-	-	-	No surgery	No surgery: suspect for late onset idiopathic generalized epilepsy	149 (15)
8	M/6	R/Parietal	Multifocal gliosis, R more than L	R central paramedian	R central paramedian	R frontal or parieto-occipital	-	No surgery	No surgery	77 (19)
9	M/15	R/Parietal	MTS suspect	R hemisphere, most temporal	R centro-temporal	R temporo-parieto-occipital	R temporo-parietal	Occipital gliosis. Hippocampus: MTS (Wyler grade IV, ILAE grade 1)	Resection of focus occipital right and removal of hippocampus. Seizure free 2 months.	183 (21)
10	M/14	R/Temporal	FCD	R posterior temporal	R posterior temporal	R posterior temporal	-	FCD 2A	R occipito-temporo-basal resection, seizure free 6 months	2 (1)

Table 1: Characteristics of all included patients, showing the MEG affected region (side/location), MRI abnormalities, interictal and ictal EEG findings, PET and ictal SPECT findings, pathology and surgery information and the number of marked HFOs followed by the number of 'HFO moments', time points where HFOs occur simultaneously. M: male, F: female, L: left, R: right, SEGA: subependymal giant cell astrocytoma, FCD: focal cortical dysplasia, MTS: mesiotemporal sclerosis, - (dash): information not available or modality not used in pre-surgical workup. Patient 1, 7, 11 and 12 are not included in this table because no visual HFOs were present in the MEG recording

5 Optimization of MEG data and beamformer analysis

5.1 Introduction

This chapter will introduce the pre-processing and spatial filtering techniques used in this thesis. After that, the methods used to compare these different filtering techniques are explained, and the results of the comparison are presented.

5.2 Spatial filtering of MEG data

To be able to distinguish HFOs from background noise, a good signal-to-noise ratio (SNR) is needed. Noise can be attenuated by application of signal space separation (SSS) to improve the SNR of MEG recordings. The SSS algorithm breaks down the measured magnetic field in separate components for sources of activity present in and around the MEG. It has been found empirically that the measured magnetic field is typically created by around 150 different sources [35]. Since the MEG has 306 channels to measure the magnetic field, the magnetic field is oversampled. Because of this oversampling, all the significant sources in and around the MEG can be modelled mathematically by a linear expansion of spherical harmonic functions. This leads to an equation where one part of the expansion diverges towards the center of the head, meaning that these sources are located inside the brain (internal components, green in figure 6). The second part of the expansion diverges towards infinity, outside of the head, and thus represents sources outside of the MEG measurement setup (external components, red in figure 6). The signals coming from outside sources can be discarded before reconstructing the signal. Note that the internal and external components are orthogonal.

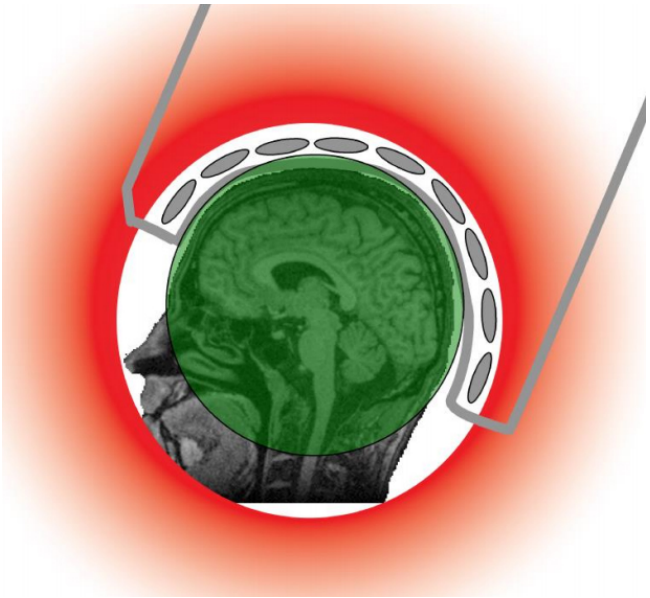

Figure 6: Example of Signal Space Separation (SSS). Sources in the green sphere are of interest. The red sphere contains external interfering sources. SSS separates these sources and discards the sources in the red sphere. Figure courtesy of J. Nenonen, Elekta Neuromag Oy.

One disadvantage of SSS is that it is unable to determine if a source is inside or outside the head when the source is very close to the sensors. Removal of these signals is accomplished by applying an extension on SSS called spatio-temporal SSS or tSSS. This algorithm checks if the aforementioned inside and outside part of the expansion contains common components over time. Imperfect separation of internal and external components, typically for noise sources close to the sensors, lead to common signals in the inside and outside expansion, which may be detected by simple correlation, and subsequently be removed. [36].

5.3 cxSSS

Recently a new pre-processing algorithm has been proposed by Elekta, the manufacturer of the MEG system, called cxSSS, which is an abbreviation for covariance-based (c) and uncorrelated noise subtracted by cross-validation (x) extension of SSS (see figure 7). The new algorithm adds steps to the already existing noise suppression algorithm. The first step removes the head localization coil signals by applying a notch filter for the frequencies used by the head localization coils (around 300 Hz). The second step calculates the uncorrelated noise for each sensor. The SSS model is constructed as described before, but one sensor is excluded from the model. The constructed SSS model is used to estimate the signal of the excluded channel. The estimation of the signal of the excluded channel is then subtracted from the signal of the excluded channel itself, and the result is the uncorrelated, sensor specific noise. This process is repeated for all MEG sensors. After this step the uncorrelated noise is visually inspected and a list of bad channels is saved for use in further processing. In the next step the correlated artefacts are removed from the signal using tSSS as described above. The channels marked as bad are not considered for the construction of the SSS model when applying tSSS filtering.

The previously mentioned steps are also applied to an empty room MEG recording, ideally of the same day as the recording of interest. After these steps there is the original recording and the empty room recording, both cleaned of correlated noise using tSSS, and for both recordings a list of bad channels. The list of bad channels was limited to 12 channels per recording because the next steps of the analysis need a minimum number of active channels in the recording to function.

The tSSS filtered empty room recording is used to calculate the noise covariance matrix. Since this information is based on the empty room recording, the noise present in this recording is specific for the MEG system. The noise covariance matrix represents an estimation of the noise level and the relation of the noise between all sensor pairs. This information is used to improve one of the last steps of the filtering process where the data covariance matrix is inverted. Very small values in the data covariance matrix can turn into very large values by the inversion step. To prevent this, it is common to add noise to the data covariance matrix. The cxSSS algorithm uses the information in the noise covariance matrix to add noise to more specific values of the data covariance matrix, increasing the signal quality by improving the numerical accuracy of the matrix inversion. This is performed in the last step of the cxSSS algorithm, alongside the removal of the uncorrelated sensor noise. A comparison for the effect of SSS and cxSSS on raw data are presented in figure 8.

5.4 Beamforming

Beamforming is a filtering technique, which can be compared to frequency filtering, but for spatial locations. This technique can be used after previously mentioned pre-processing techniques. The beamformer reconstructs the strength of a neuronal signal at a specific location in the brain as the weighted sum of all the MEG channels. For each point of interest in the brain a weighing factor is calculated for every MEG sensor [1, 17, 44]. The weights are optimized for each region sequentially to remove signals from noise sources (including interfering signals from other brain regions), but to retain the signal from the location of interest. By applying the weights to the MEG sensors, a time trace can be constructed for each specific location in the brain, a virtual sensor (VS) [17]. This process is schematically explained in figure 9.

The beamformer weights are calculated based on the power of the signal, represented by the covariance matrix (C), which is calculated over (a selection of) the signal. The length of the signal used to calculate the covariance matrix is called the integration window (T_{cov}). Brookes *et al.* looked at the influence of integration window T_{cov} and the bandwidth of the signal (BW) on the beamformer result [7]. For evaluation of the beamformer they looked at the covariance matrix error (ΔC), which is the difference between an analytical derived covariance matrix and a data-derived covariance estimate. Using ΔC, the Frobenius norm was calculated which represents the total error in the covariance estimate across all MEG channels. It was found analytically that the Frobenius norm of the covariance matrix error follows the formula:

$$\|\Delta C\|_F = \nu^2 M \sqrt{\frac{2SNR + 1}{2T_{cov}BW}} \tag{1}$$

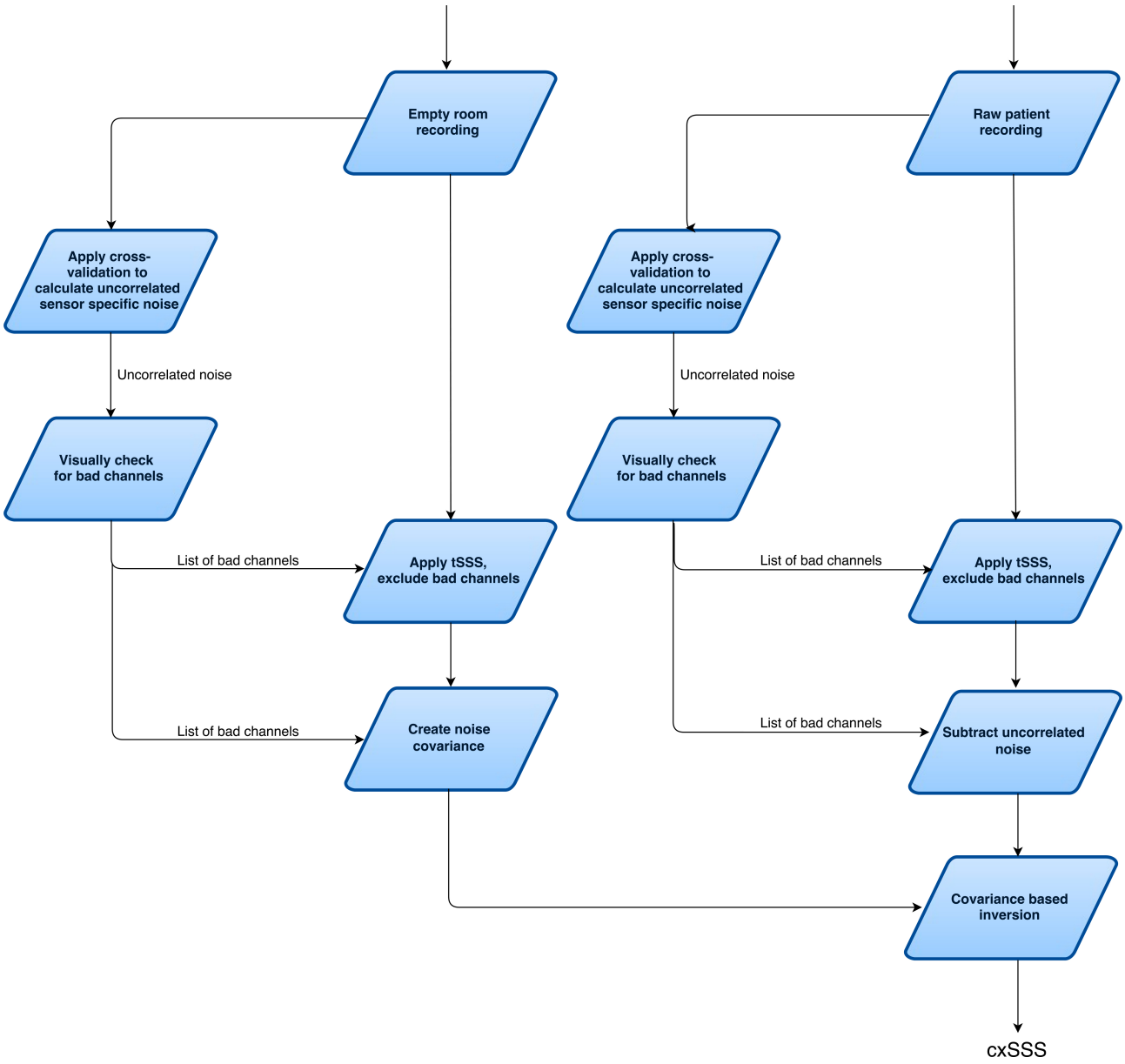

Figure 7: Schematic explanation of the cxSSS algorithm. Two files are used as input, the patient recording and the empty room recording. Bad channels are visually inspected based on the uncorrelated noise. These channels are excluded for the rest of the analysis. tSSS is performed, the uncorrelated noise is subtracted from the patient recording. The noise recording is used to calculate the noise covariance. This noise covariance is used to improve the inversion. The result is the patient file containing less correlated and uncorrelated noise compared to the original (see figure 8).

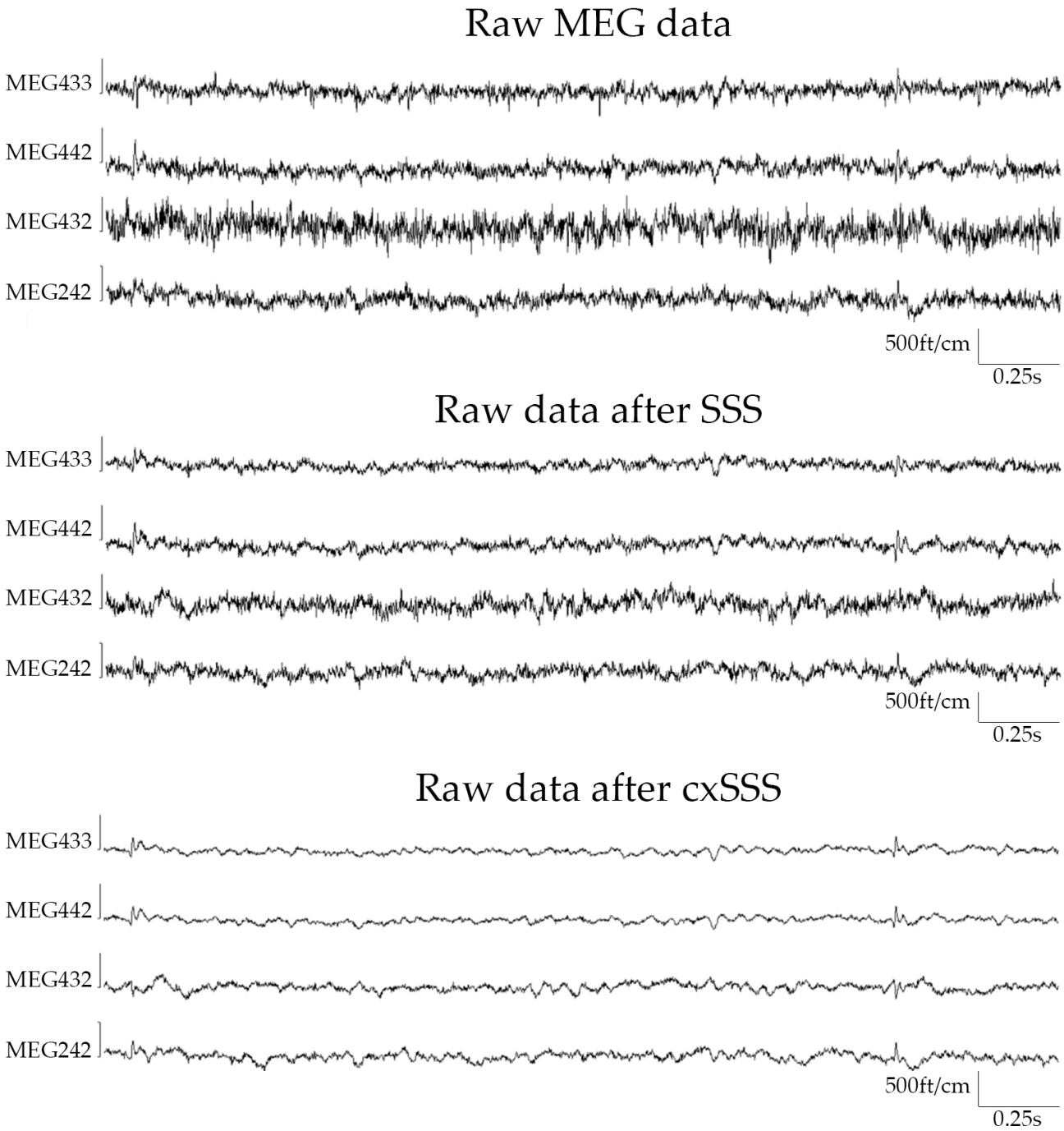

Figure 8: Example of the effect of SSS and cxSSS. This figure shows four traces of unprocessed MEG data at the top. The same four traces are shown in the middle after applying SSS. The traces at the bottom show the result of applying cxSSS on the raw signal. The cxSSS algorithm is able to improve the quality of the signal substantially when compared to the result of SSS. Figure courtesy of J. Nenonen, Elekta Neuromag Oy.

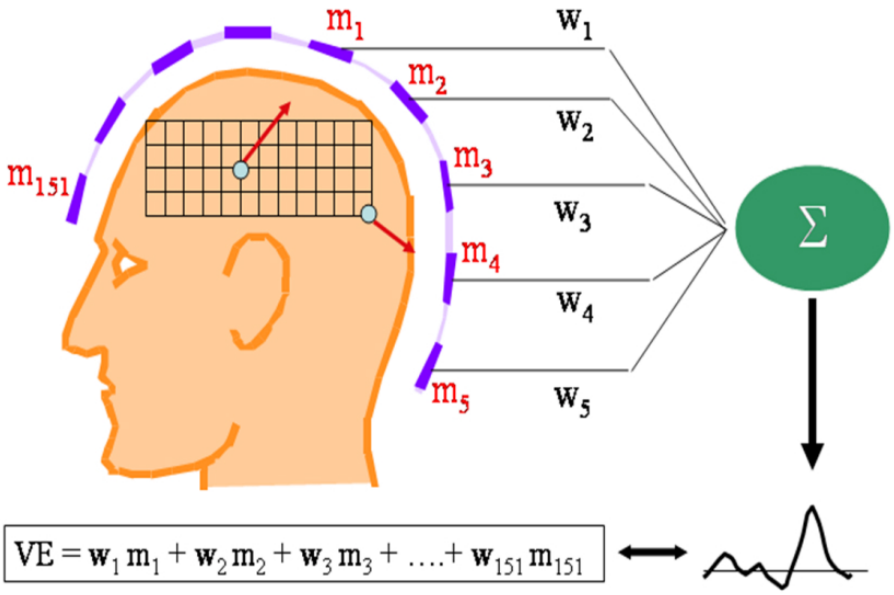

Figure 9: Beamformer analysis. A weighing factor (w) optimized to minimize the influence from sources not located in the target location is applied to the MEG sensors output (m) to produce a signal containing only activity from the target area. The result is called a virtual sensor (VS) or virtual electrode (VE). Figure courtesy of D. Cheyne, University of Toronto.

where $\|\Delta C\|_F$ represents the Frobenius norm of the covariance matrix error, v^2 the noise power in all MEG channels, M the number of MEG channels, SNR the signal-to-noise ratio averaged over all channels, T_{cov} the integration window and BW the bandwidth of the signal. Of these parameters T_{cov} and BW are the most interesting, because they are free to choose, while the other parameters are fixed properties of the signal and the MEG setup.

The method used by van Klink *et al.* has a limited T_{cov}, because only 200ms windows around the spikes are considered for calculation of the data covariance. If there are few spikes, T_{cov} will be small and thus, according to formula 1, the total error in the covariance estimate will be high. The bandwidth used in the study by Van Klink *et al.* was 80-500 Hz. Analysis of the raw MEG recording showed constant activity at 300 Hz. This activity was caused by the head localization coils, used to track the movement of the head during the recording. This led to the idea to investigate the influence of changing the BW settings in the beamformer.

5.5 Methods

5.5.1 Adaptation of beamformer settings

The settings of the beamformer algorithm were changed in an attempt to improve the SNR. The T_{cov} was increased by using the full length of the signal. A secondary advantage of using the whole signal was that there was no longer a need to mark spikes in the physical sensor data. Two settings were used for BW, the standard 80-500 Hz and 80-250 Hz to avoid the 300 Hz head coil activity. These settings were compared to the already existing set, which used 80-500 Hz as BW, but restricted the T_{cov} to a 200 ms window around spikes. These settings were used for all 12 patients, where tSSS was used for pre-processing. This lead to a total of 3 T_{cov}/BW settings:

- T_{cov} restricted to a 200ms window around spikes marked on the MEG channels, with BW restricted to the 80-500 Hz band.
- T_{cov} unrestricted, so the total recording is used, BW restricted to 80-500 Hz.
- T_{cov} unrestricted, BW restricted to 80-250 Hz band to avoid the head localization coil signals.

The adapted beamformer algorithms ran on all 12 patients of the study by Van Klink *et al.*, as visually marked HFOs were available in this dataset for comparison between different settings. VS were calculated at the same locations in the brain as in the study by Van Klink *et al.*, which enabled direct comparison of the new and original beamformer algorithms.

The SNR was calculated for each channel with HFOs in each patient with HFOs, since marked HFOs are needed for the SNR calculation. Parts of the signal not marked as HFO are used as noise and all marked HFOs are used as signal. The SNR was calculated by the average power in the HFO band (80-500 Hz) for the marked HFOs, divided by the average power in the same frequency band of the rest of the signal, for each channel. The SNR for each channel was then compared to the SNR of the same channel in the same patient, but with different beamformer settings.

Statistical analysis using regression was performed to test if there was a significant difference between the three different beamformers. Three things had to be considered in choosing the right model for this dataset.

- Each patient had 70 channels where the SNR could be calculated if there was at least one HFO found. Since the majority of channels did not show HFOs, the dataset has missing data. This can be solved by removing all missing data, or by imputation, where the know data in the set is used to estimate the missing data. Since there is only a small amount of known data, it was chosen not to use imputation.
- If there is much variation in the relation between the beamformer and the SNR for each patient, the statistical model can be improved by adding a term to model this variation. The need for such an extra term was evaluated by comparing the regression lines for each patient. These regression lines are based on the scatterplot of the SNR versus patient. Based on the similarity of these plots it was decided that correction for the variation in the relation between the beamformer and the SNR per patient was not needed.
- If there is a correlation between the SNR of neighboring channels the measurements are not independent identically distributed. This leads to a more significant outcome. This can be corrected by supplying the correlation structure to remove the correlation. Since there are many more channels than there are data points, the correction for correlation would be too strict, and so it was decided not to correct for correlation. Bootstrapping was used as an alternative to correlation correction.

Statistical analysis of the data was performed using SPSS version 22.

5.5.2 tSSS and cxSSS

To see if the combination of cxSSS and beamforming outperforms the combination of tSSS and beamforming, the best beamformer setting was used to construct VS based on cxSSS. The SNR of the result was compared with the SNR of the tSSS pre-processed data using the same beamformer settings.

5.6 Results

At the time of writing it was found that there were problems with the cxSSS algorithm which was used for the processing of all 12 patients. It turned out that the cxSSS algorithm contained a bug that introduced artefacts to the signal. An example of this is shown in figure 10. A new version of the software where this bug is fixed is not available at the time of writing this report. Elekta was so kind to send a copy of one patient file (patient 9), where they applied all the cxSSS steps using a workaround. This file is used for the results section to show what is possible with this new algorithm. This means that for the comparison of the different beamformer settings the data from all patients described in chapter 4 is used, but that the comparison between tSSS and cxSSS is based on one patient.

5.6.1 Adaptation of beamformer settings.

The SNR was calculated for eight patients, with an average number of 72 marked HFOs. The statistical analysis showed there was no significant difference between the 3 beamformers ($p = 0.119$). Boxplots for the SNR for every patient-beamformer combination are shown in figure 11. Details for one patient (patient 9) are shown in figure 12. This figure shows the difference in SNR per channel, between the windowed beamformer

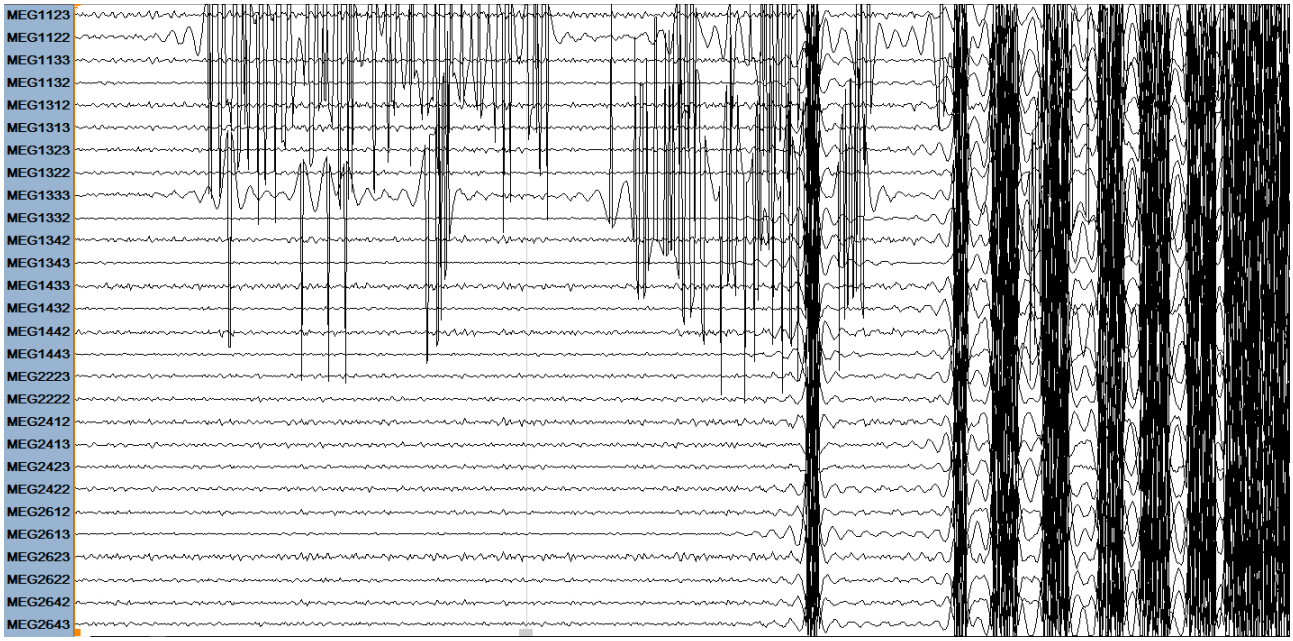

Figure 10: Example of 0.8 s of data where artefacts are introduced to the signal by a bug in the cxSSS algorithm.

and the beamformer over all data, both using tSSS as pre-processing. The number of HFOs per channel is indicated by the number on top of the bar. Positive numbers indicate better results for the beamformer based on all data, and negative numbers indicate better results for the windowed beamformer. Figure 12 shows that using the all data beamformer decreased the SNR in 15 channels, while it increased the SNR in 28 channels compared to the window beamformer. It is noteworthy that 8 of the 15 channels where the SNR decreased were located in the control side of the brain (channel 1-35 are control in this patient), where HFOs were not expected. Only one HFO was found in these channels. An example of the time traces for channel 14, where the SNR difference is negative, and channel 67, where the SNR difference is positive, is shown in figure 13.

Channel 14 (top pair of traces) shows that this HFO is visually better detectable in the window beamformer. Channel 67 (bottom pair of traces) shows that the HFO is more clear in the beamformer using all data. Another important thing to note is the noise preceding the HFO in channel 67 was reduced with the new beamformer, which probably caused the large improvement of the SNR. It was not possible to determine the best beamformer based on statistics over all patients, but visual inspection of the data showed less noise when using the beamformer based on all data for the covariance estimation, and this effect was most visible in the affected brain region, i.e. where most HFOs are expected. Based on this information it was chosen to use the all data beamformer for the comparison between the different pre-processing techniques.

5.6.2 tSSS and cxSSS

After comparing the influence of the bandwidth and the length of the data covariance matrix, the best beamformer was used to compare two pre-processing techniques tested on the same data set. This was done to determine if the new pre-processing algorithm as described in the methods performed better compared to the already existing pre-processing algorithms. The result of the comparison is shown in figure 14. This figure shows a boxplot of the SNR for both pre-processing techniques using the same beamformer. The cxSSS pre-processing algorithm yields a higher SNR than tSSS, the currently standard used algorithm. A paired sample t-test between the two pre-processing algorithms shows a significant improvement in SNR ($t(df) = 32$, $p<0.0001$). Details of the difference in SNR per channel are shown in figure 15. This figure shows that the SNR for cxSSS increased in 38 out of 42 channels when compared to the SNR for tSSS.

For comparison the same HFO locations and channels as shown in figure 13 for the comparison of the window and all data beamformer are shown in figure 16 for the tSSS and cxSSS pre-processed data. Channel

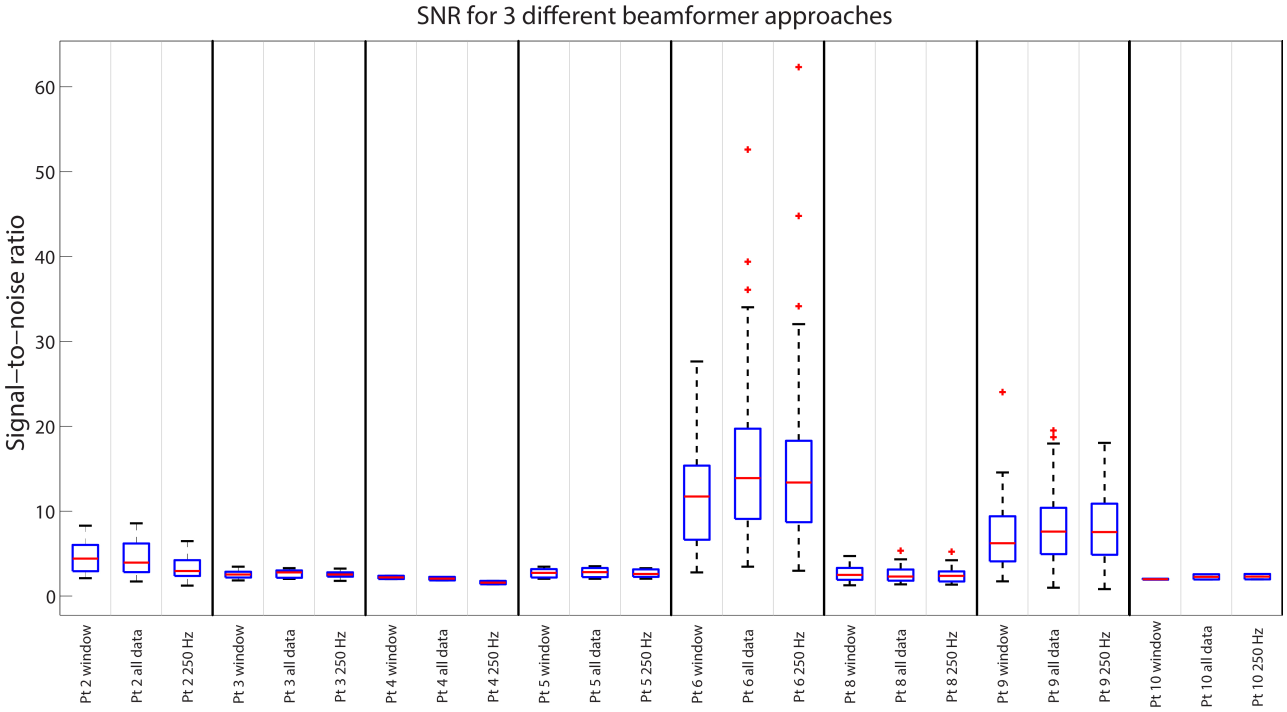

Figure 11: A summary of the calculated SNRs per patient, for the beamformer using a 200ms window around marked spikes as integration window T_{cov} (termed 'window'), for the beamformer using all data as T_{cov} (termed 'all'), and the beamformer using all data as T_{cov}, but with a bandwidth limited to 80-250 Hz (termed '250 Hz'). The results are shown in triplets, where the beamformer based on the 200ms window is on the left, the beamformer based on all data on the middle and the beamformer with the limited bandwidth on the right. It can be seen that the beamformer based on all data shows SNR values that are roughly the same or slightly higher than the other beamformers.

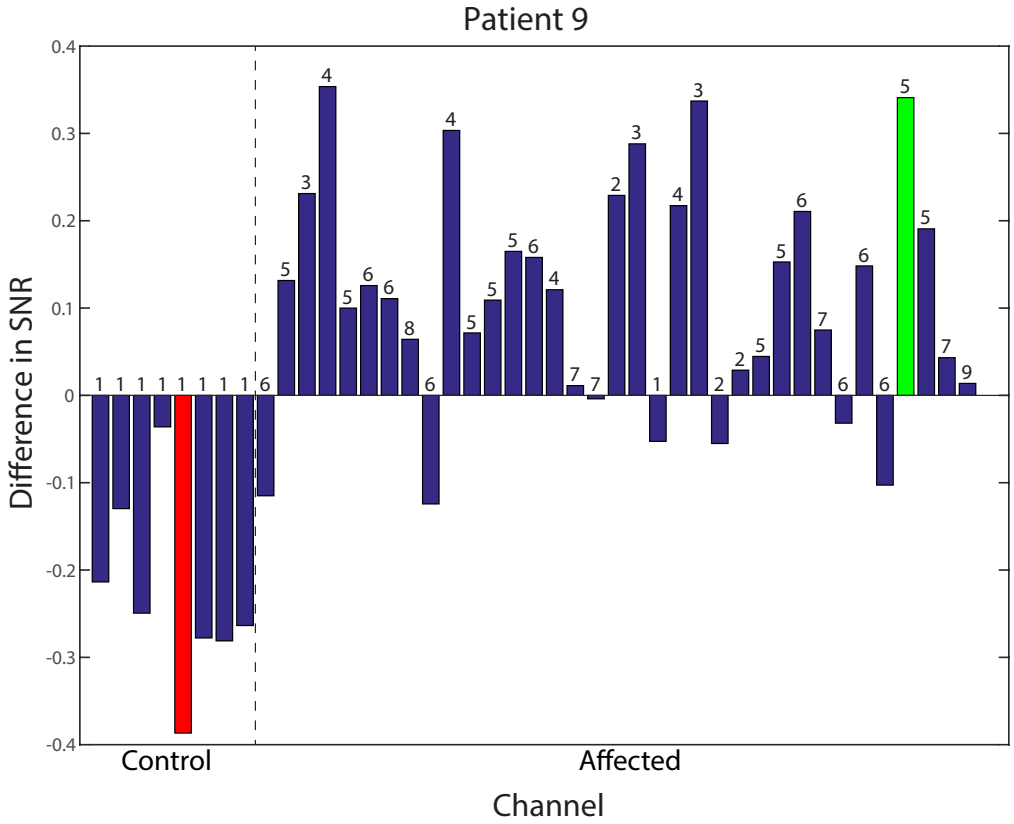

Figure 12: Example of the difference in SNR for each channel of patient 9 containing HFOs, calculated as the ratio of the difference in SNR normalized by the total SNR calculated as $(SNR_{all} - SNR_{window})/(SNR_{all} + SNR_{window})$. The numbers on the bars indicate the number of HFOs present in the channel and thus used for calculation of the SNR for the channel. Channels to the left of the vertical dashed line are located on the control side of the brain, channels to the right of the vertical dashed line are on the affected side of the brain. Details for the bars in red and green are shown in figure 13.

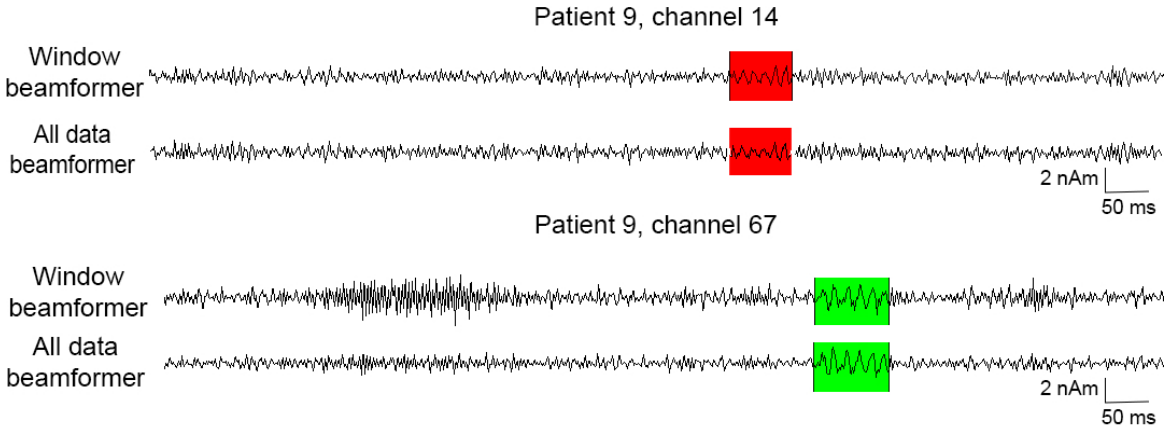

Figure 13: Virtual sensor output showing the effect of the different beamformer settings. All data shown is 80 Hz high-pass filtered. The top pair of traces shows the same epoch for the same channel (channel 14 in figure 12). The first trace is the result of the window beamformer, the second trace is the result of the beamformer on all data. In this example, the window beamformer seems to show a more clear HFO (marked in red), although the difference is not very noticeable. The bottom pair of traces shows a different epoch for a different channel (channel 67, green, in figure 12) in the same patient. Again, the first trace is the result of the peak beamformer and the second trace is the result of the beamformer on all data. Note that the beamformer over all data attenuates the noise preceding the HFO.

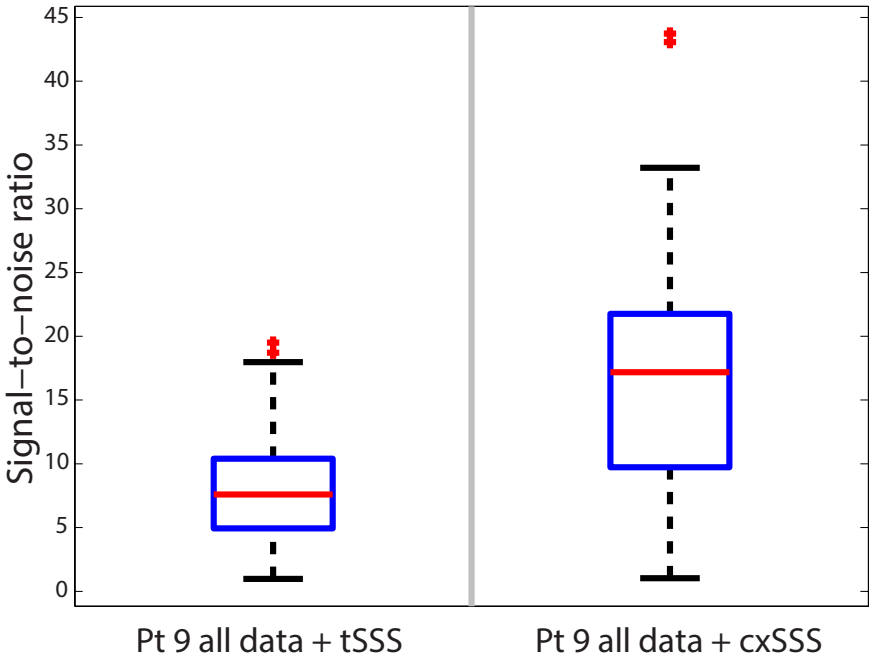

Figure 14: Boxplots showing the difference in the signal-to-noise distribution between two different pre-processing techniques, for the same dataset. The left boxplot shows the result of the all data beamformer on tSSS pre-processed data. The second boxplot shows the result of the same beamformer on cxSSS pre-processed data. The cxSSS data yields significantly better results compared to the tSSS data.

14 shows a small HFO with little deviation from the baseline when using tSSS. The same HFO was higher in amplitude when cxSSS is used as pre-processing technique. This is in accordance with figure 15, where the difference in SNR shows an increase for channel 14. Channel 67 shows a small decrease in SNR, indicating that tSSS outperforms cxSSS. This is visible in the second pair of traces in figure 16. Channel 5 and 6 are the two channels where the difference in SNR is most negative. Both channels are located on the contralateral side where no HFO activity was expected and contain only one HFO. Visual inspection shows that for both channels the small HFO that is present in the signal disappears when cxSSS pre-processing is applied.

5.7 Conclusion and discussion

In this chapter the effect of different pre-processing methods and different beamformer settings was investigated. It was shown that applying beamformer analysis on the total length of the signal instead of a 200ms window around peaks often results in signals with an improved SNR, which is mainly caused by a decrease in noise, but that there is no statistical difference between the beamformers.

Applying a beamformer with a BW of 80-250 Hz to avoid the 300 Hz activity of the head localization coil did not yield better results. This can be explained by the methods of the beamformer. As explained in section 5.4 the weights used by the beamformer are optimized to remove signals from distant noise sources. Signals can only be removed when they are included in the analysis. For this reason, trying to remove 300 Hz noise from a distant source (the head coils) is only possible when the noise frequency is included in the analysis.

Although there is no significant difference on the group level, some individual cases show a big improvement in the SNR, caused by a reduction of noise. Since the aim of this report is to automatically detect HFOs and most HFO detectors are unreliable when noise is present in the signal, it was chosen to use the all data beamformer, which showed the highest reduction in noise for most patients. Another reason to choose for the all data beamformer was that no spikes have to be marked, since no window around the spikes is used. This saves time and prevents a possible observer bias, where known information about the condition of the patient can influence the marking of spikes.

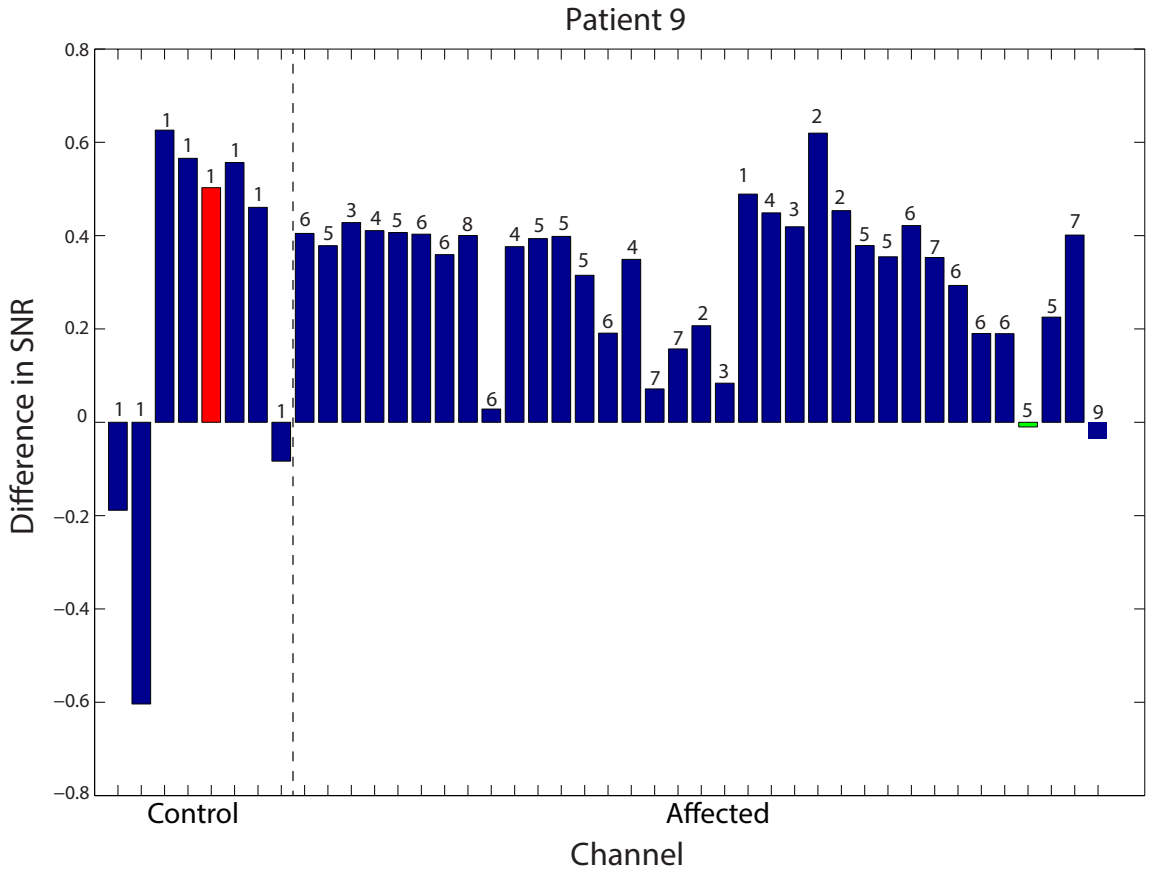

Figure 15: Comparison of the all data beamformer in combination with either tSSS or cxSSS pre-processing. The difference in SNR for each channel of patient 9 are shown, calculated as the ratio of the difference normalized by the total SNR, in formula: $(SNR_{cxSSS} - SNR_{tSSS})/(SNR_{cxSSS} + SNR_{tSSS})$. Channels to the left of the vertical dashed line are located on the control side of the brain, channels to the right of the vertical dashed line are on the affected side of the brain. The numbers on the bars indicate the number of HFOs used for calculation of the SNR for the channel. Details for the bars in red and green are shown in figure 16.

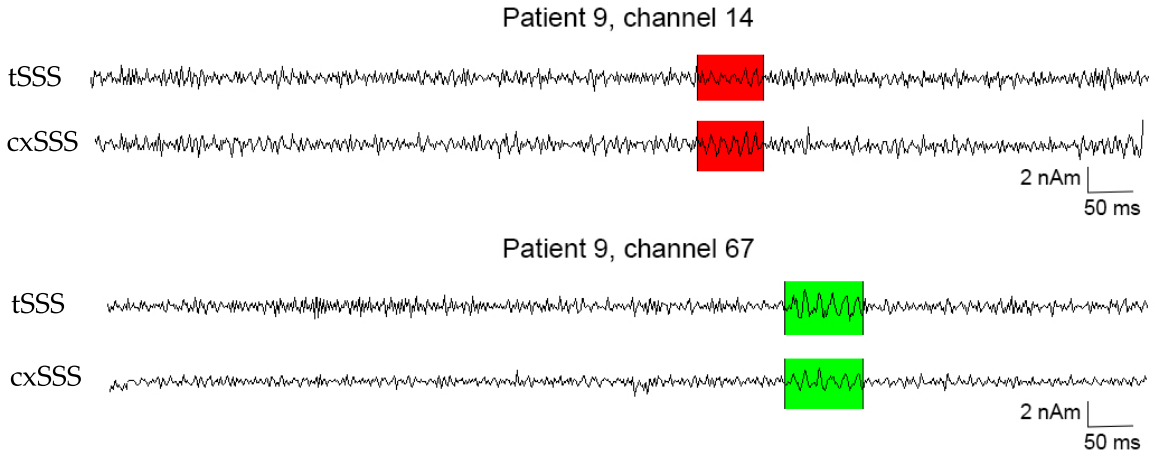

Figure 16: Virtual sensor output showing the effect of the different pre-processing techniques. All data shown is 80 Hz high-pass filtered. The top pair of traces shows the same epoch for the same channel (channel 14, red, in figure 15). The first trace is the result of the all data beamformer on tSSS pre-processed data, the second trace is the result of the same beamformer on cxSSS pre-processed data. In this example, the cxSSS trace seems to show a more clear HFO (marked in red). The bottom pair of traces shows a different epoch for different channels (channel 67, green, in figure 15) for the same patient. Again, the first trace is the result of the beamformer on tSSS pre-processed data and the second trace is the result of the beamformer on cxSSS pre-processed data. This pair of traces shows the HFO (in green) is clearer in the tSSS pre-processed trace.

The all data beamformer was used to compare the standard pre-processing technique, tSSS, with cxSSS, the pre-processing technique currently in development by Elekta. It was shown that pre-processing with cxSSS improves the SNR significantly. Analysis on channel level showed an increase in 38 out of 42 channels. Two channels showing a decrease in SNR showed the HFO disappeared when using cxSSS. A possible explanation for this is that the cxSSS pre-processing increased the SNR of the raw signal. This leads to a higher spatial resolution for the beamformer, and less leaking activity in VSs that are (slightly) misplaced from the true source location. Such counterintuitive results, a better signal leading to worse performance, have been observed previously [17, 16, 43].

This indicates a difficulty in the interpretation of the results. All manual markings of HFOs are based on tSSS data using the window beamformer. These markings are used to analyze the SNR for all settings. When an HFO disappears because the pre-processing causes less leakage of the signal to neighboring regions, the SNR decreases whilst the result is actually better (in terms of spatial resolution). This can be solved by visually marking HFOs in both the tSSS and the cxSSS data. This also avoids the possibility of missing HFOs that are visible in the cxSSS data but not in the tSSS data.

The analysis of the cxSSS pre-processing was performed for one patient. Although this patient showed a significant increase, no firm conclusions on the cxSSS algorithm can be made before a new version of the software is released and all patients are analyzed.

6 Optimization of the HFO detector

6.1 Introduction

Currently few (semi-)automatic detectors for HFOs are available, and most of them are created for HFO detection in intracranial grid- or depth-electrodes. To detect HFOs in MEG, a detector needs to be able to work with noisy signals because of the low SNR of MEG compared to intracranial recordings. For the same reason, the detector should be able to detect HFOs that do not rise above the rest of the signal as clearly as HFOs do in intracranial data.

One of the first detectors for HFOs was based on the root means square (RMS) of filtered intracranial EEG signal [32]. An epoch was considered an event of interest (EOI) if the RMS value was higher than five times the standard deviation (SD) of the RMS of the whole signal and the rectified signal displayed 6 peaks higher than three times the SD of the rectified signal. All EOIs had to be visually reviewed to discard artifacts. It was reported that this algorithm finds 84% of the HFOs found by visual scoring, but only after the visual inspection of all EOIs. An overview of these steps is shown in figure 17. Over the next years this energy-threshold method was repeated with another method: the Hilbert transform [10] which creates an envelope over the contour of the signal. This envelope is related to the RMS of the signal, and is used in the same way for detecting EOIs. This detector was only used to help with visual reviewing, and no sensitivity of specificity values were given. The second generation of HFO detectors focused more on the oscillatory characteristics

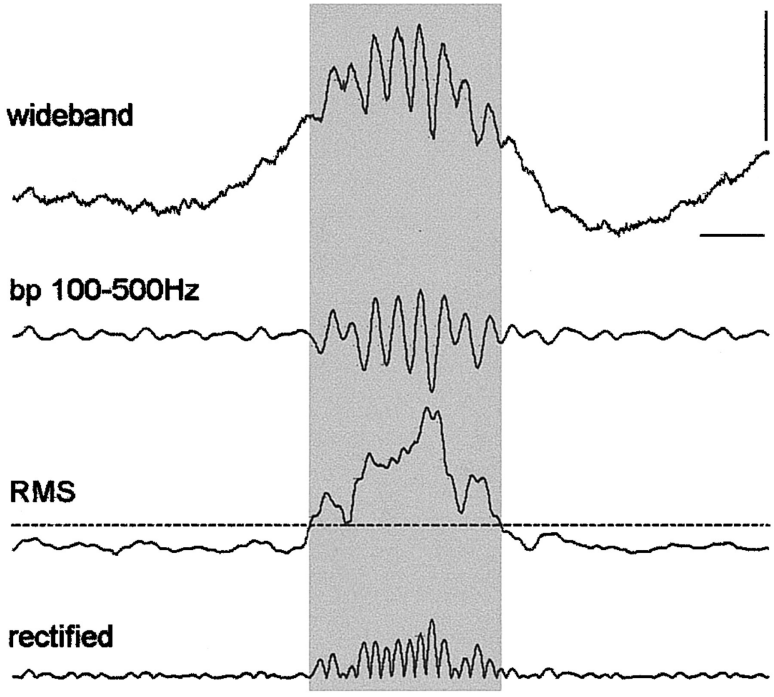

Figure 17: Example of the steps used by the detector designed by Staba *et al.* [32]. The wideband signal is bandpass filtered between 100-500Hz, the RMS is calculated over the resulting signal and a threshold is set at 5 standard deviations for the detection of potential HFOs. The detected potential HFO signal is rectified to check if there are more than 6 peaks present that rise 3 standard deviations above the baseline. Horizontal calibration bar: 5 ms, vertical calibration bar: 0.5 mV. Figure adapted from [32].

of the HFO in combination with the energy methods described above. A detector for HFOs in depth EEG electrodes developed by Zelmann *et al.* [50] did this by looking at the entropy of the signal, where high entropy indicates 'randomness' of the signal and low entropy indicates oscillatory behavior. They determined 'baseline' signal and EOI epochs based on the entropy. Subsequently the energy threshold which had to be exceeded for an EOI to be identified as HFO was based on the energy of the baseline present in the analyzed epoch, so signal variations over time are taken into account, which mimics visual scoring. The study reports a sensitivity of 96.8% and a specificity of 95.1%. It should be noted that this extreme specificity is due to the fact that only the EOIs which corresponded to a visually marked HFO or baseline were considered.

The first detector build for non-invasive EEG recordings was developed by von Ellenrieder *et al.* [42]. This detector uses the fact that HFOs are oscillations in a narrow frequency band. The detector analyzes the signal in narrow frequency bands of 10Hz and in a broad frequency band. When the RMS in one or more of the frequency bands is higher than a threshold for a set duration, the event is marked as potential HFO. If the potential HFO shows activity in multiple narrow frequency bands as well as in the broad frequency band, it is considered an artifact. The potential HFOs are split in true and false positives by using a classifier. The classifier used two features: the ratio of the maximum absolute value of the broadband signal to the maximum absolute value of the signal in the frequency band in which an event was detected, and the maximum value of the RMS of the narrow band signal of the frequency in which an event was detected. These two features were compared to HFOs marked by an expert, to determine the best values for the two features, which makes this a semi-automatic detector. A sensitivity of 95% and a 40% positive predicted value was reported for this detector.

All of the above detectors have a very high sensitivity, but at the cost of many false positives. Because of the high amount of over detection, there still is a need to visually verify the HFOs identified by these detectors. We require a detector that is able to analyze a large amount of data, is fast, able to run unsupervised and able to handle low-SNR MEG data. The detector of Burnos *et al.* seems the most suited for this task, because it uses an unsupervised 2-step algorithm where both steps can be optimized for MEG data [8].

The paper by Burnos *et al.* describes the working of the detector as follows. First the EEG signal was band-pass filtered for the frequencies of interest (80-500Hz). This was done using an infinite impulse response (IIR) Cauer filter with 60 dB minimum lower/upper stop band attenuation, 0.5 dB maximum pass band ripple and 10 Hz lower/upper transition. The signal was forward and reverse filtered to avoid phase distortion. The choice for an IRR filter was based on computational speed and the sharp cut-off.

A Hilbert transform (envelope) was applied and the standard deviation of the Hilbert transform was calculated over the first 5 minutes of the signal (figure 18A). A threshold was set at the mean of the Hilbert transform plus 3 standard deviations, based on these first 5 minutes. When the envelope reached values above this threshold, and if the duration of this event was more than 6ms, it was marked as an EOI.

The version obtained from Burnos *et al.* to use for this project had a different approach for finding EOIs. Instead of using the standard deviation of the Hilbert transform for detecting EOIs, the new version used the entropy of the signal combined with the Hilbert transform. The new algorithm works as follows. The entropy is calculated for every sample of the first 60 seconds of the signal. For every second the corresponding maximum entropy is calculated as well. High entropy signals can be seen as 'random', with equal power in all frequency bands, whereas low entropy signals are not random but oscillatory. This information is used to detect parts of the signal containing 'baseline', since the baseline signal is assumed to be more 'random' in comparison to an HFO, which oscillates at a certain frequency. A percentage of the maximum entropy, set by a pre-specified parameter, is used as a threshold to detect samples of the signal with high entropy. For all samples with high entropy the corresponding value of the Hilbert transform (the height of the envelope) is stored in order to build an empirical cumulative distribution function. This function shows the distribution of the stored values, and is used to look up what Hilbert transform value is equal to or larger than a certain percentage (set by a parameter called *CDF*) of all baseline samples. This is done to reduce the influence of baseline segments that correspond to a very high Hilbert transform value. The Hilbert transform value corresponding to this *CDF* parameter is used as threshold for the total signal. Every epoch above this threshold that lasts longer than 6ms is considered an EOI. If the time between two EOIs was less than 10ms, the events were merged.

In the second step, the EOIs were checked for the presence of HFOs. The HFOs were assumed to be short-lived events with a spectral peak at a distinct frequency. To check if EOIs were matching these assumptions the EOIs were evaluated in time-frequency space by using a Stockwell transform [33]. The Stockwell transform uses a frequency dependent window width to increase the time-frequency resolution and thus gives a better peak sharpness compared to the short-time Fourier Transform. An example of the resulting spectrum is given in figure 18B. A power spectral density curve (PSD), as shown in figure 18C, was created for every time sample in a 1 second window around the maximum value of the Hilbert envelope of the EOI (the gray

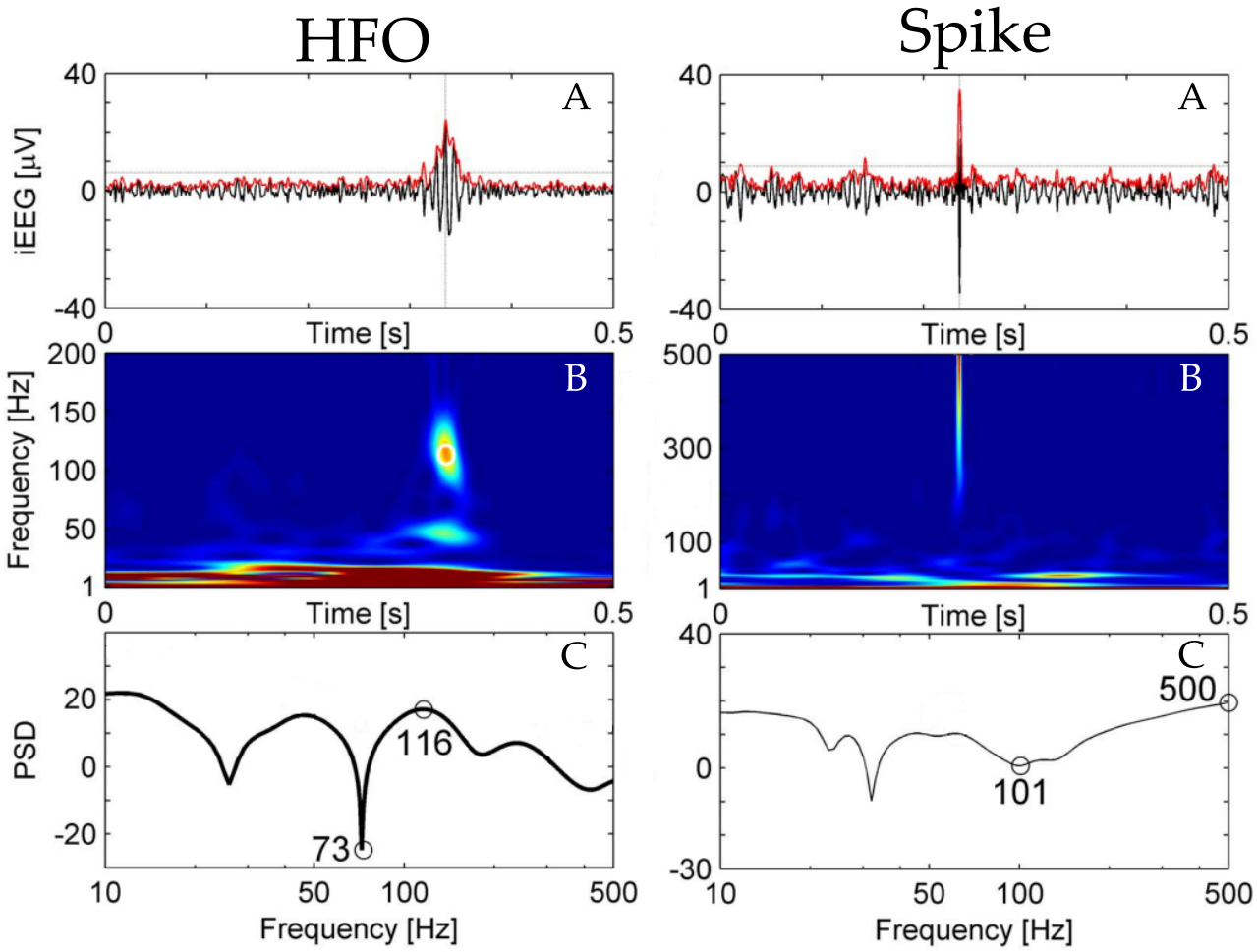

Figure 18: HFO detection algorithm as designed by Burnos *et al.* [8]. The left column shows the detection of an HFO, the right column shows the rejection of a spike. A: Example of the Hilbert transform of the filtered signal. When the Hilbert transform is higher than the threshold (grey horizontal line) for a pre defined amount of time the event between the upward and downward crossing of the threshold is considered an event of interest (EOI). These EOIs are used for further processing. B: The spectrogram of the same data as A, made using the Stockwell transform. C: The PSD of one sample of the HFO/spike. This figure shows the PSD of the sample indicated by the grey vertical line in A. Because the example of the HFO has a peak at 116 Hz and a trough at 73 Hz, and the ratio between this peak and trough is sufficient, this sample is considered an HFO. The spike however displays the peak at the maximum frequency of the spectrogram (500 Hz in this example) and is rejected. An HFO is marked in the signal when at least 0.1 s of consecutive samples are considered as HFO. Figure adapted from [8].

vertical line in figure 18A).

The PSD of an HFO was assumed to show a high frequency peak (HiFP), separated from a low frequency peak (LoFP) by a spectral trough (Trough), an example is given in figure 18B. The high frequency peak is the maximum power found between 60Hz and 500Hz, where the 60Hz boundary is chosen to exclude power line artifacts. The trough is the minimum between 40Hz and the spectral peak. With these 3 points, an HFO had to satisfy the following criteria;

1. The trough should have a sufficient depth, defined as a ratio:

$$depth = \frac{power(Trough)}{power(HiFP)} < 0.8$$

2. The event must show a sufficiently high HiFP, defined as:

$$peak = \frac{power(HiFP)}{power(LoFP)} > 0.5$$

3. These two conditions must be satisfied for at least 11 samples (upwards rounding of 0.026s x sample frequency, 1024 Hz in this case).

If these conditions were satisfied, the EOI was considered to be a true HFO. Especially the high specificity of the second step and the possibility to add rules based on the spectral content of the signal made that it was chosen to modify the Burnos detector for this project. Comparing this detector to the ones previously published is difficult because no expert marked HFOs were used to calculate sensitivity and specificity values in the previous studies. The overlap between the locations of channels containing HFOs and the location of the SOZ estimated by the pre-surgical workup was used to assess the performance of the detector. Burnos *et al.* report the results for 6 patients, with a mean sensitivity of 53.5% (SD: 33%) and a mean specificity of 85.5% (SD: 23.0%), where it should be noted that the specificity in 5 out of 6 patients was above 90%.

6.2 Methods

Chapter 2 showed what method should be used to get the highest SNR. This section describes how the settings of the Burnos detector were changed for optimal detection in the optimized data. First it is described what changes were made to the original Burnos detector as described above, and second it is described how the parameters of the detector were optimized for this study.

6.2.1 Detector parameters

The Burnos detector has many parameters that can be changed. Only the most important parameters are explained. First are the filter settings for the high- and low-pass filtering. These are used for the bandpass filtering as explained earlier. Next are the settings for the detection of EOIs and HFOs. *BLst_freq* indicates the lowest frequency where the algorithm should look for baseline. Since only HFOs frequencies are of interested, this parameter was set to 80Hz. The parameter *dur* is used to indicate for how many seconds the detector has to search for baseline samples before continuing to the next step. *BLmu* sets a limit for the detection of baseline. It was used to indicate the value, as a percentage of the maximum entropy, which should be exceeded for a sample to classify as baseline. This parameter also influences the *CDFlevel* parameter, which determines where the cut-off value for the cumulative density function is placed, as described earlier in this chapter. Both *BLmu* as *CDFlevel* were optimized with a custom made Matlab algorithm (see next section). The parameter *maxIntervalToJoin* indicated the maximum interval between EOI detections that were merged. All EOIs closer to each other than the value of this parameter were taken together as one EOI. This interval was set to 10ms.

The following parameters are used in the second step of the detector where, in summary, for every sample of an EOI a PSD was calculated, and the peaks and troughs of this PSD were calculated. An HFO should have a peak in the HFO band of which the frequency boundaries are set equal to the bandpass filter frequencies. To exclude artefacts the HFO peak should be separated from the lower frequencies and should be higher

than 40Hz, indicated by the *bound_min_peak* parameter and with a maximum of the HFO peak frequency. To check if the distance between the height of the peak and the depth of the trough was sufficient, the ratio between the peak and trough was calculated. If this value was higher than the *min_trough* parameter, which was set to 0.1, the sample was counted as a true HFO sample. If the algorithm found consecutive HFO samples for at least the duration of the *min_HFO_duration* parameter which was set to 0.025 based on literature and inspection of the data, it was marked as a true HFO.

After running the detector with the parameter settings described above, the result of the detector on MEG data was not satisfactory. Since the Burnos detector was built for the detection of HFOs in invasive EEG data, it needed modification to work on MEG data. The following adaptations were made:

1. The Burnos detector uses the Hilbert transform on the positive peaks of the signal only. This is a problem for HFOs in MEG because these sometimes deviate from the background only towards negative values, so at the negative peaks. To solve this, EOIs were detected first for the Hilbert transform over the positive peaks, then for the Hilbert transform over the negative peaks, and then merged together.
2. The detector was adjusted to ignore high frequency peaks around 150Hz, since there was a power line harmonic present at this frequency. It was decided not to ignore peaks around 100Hz, since this is the frequency where most HFOs were found in the study by van Klink *et al.*
3. A custom script was written to compare the mean of the absolute value of the EOI to the mean of the absolute value of the signal surrounding the EOI. This was done by calculating the mean and standard deviation (SD) of the EOI and 1000 samples preceding and following the EOI. If the mean+SD of the samples preceding or following the EOI was higher than the mean of the EOI, the EOI was dropped from the analysis.
4. Custom scripts were written to visualize the EOIs and detected HFOs in reviewing software (Stellate Harmonie), and to merge these EOIs and detections with the previously visually scored data.

6.2.2 Optimization of the parameters

Two of the parameters described above, *BLmu* and *CDFlevel*, are not described in literature for MEG data. First it was tried to find the optimal settings for these parameters through optimization. This was done using a custom Matlab script, which ran the detector for 8 data sets (for the 8 patients who showed visual HFOs), with varying settings for the *BLmu* and *CDFlevel* parameter. The script compared the visually marked dataset used by van Klink *et al.* to the automatic detections for every combination of the parameters. This resulted for every patient and parameter combination in a total number of EOIs, total number of automatic detected HFOs, number of true positives defined as the number of overlapping automatic detections with visually scored detections, number of false positives defined as automatic detections not overlapping with a visual detection and false negatives, defined as a visual detection not detected by the automatic detector. The optimization was a computational heavy process. For the comparison of 5 *BLmu* and 5 *CDFlevel* settings a desktop computer needed a week to complete the optimization.

After optimization of the detector it was found that the results were not satisfying. The results after optimization showed approximately one false positive detection every 3 seconds. To prevent this, changes to the detector were made as described above. Custom code was inserted and the combination of these custom pieces of code all yield different detection results. Optimizing for all these new settings was not feasible due to the runtime of the optimization, so another method of determining the best settings was used.

Since the obtained cxSSS file showed significantly higher SNRs compared to the tSSS file it was decided to use this file for the optimization of the *BLmu* and *CDFlevel* parameter and testing of the custom code. This was done by checking the automatic detections visually with the marked HFOs. Instead of checking separate individual detections and every individual HFO, it was decided to check for the detection of 'HFO moments'. HFOs were picked up by multiple VS at the same time and one such an occurrence was considered as one HFO moment. All custom code and parameters were set to their least strict settings and the resulting detections were visually inspected. At the least strict settings almost the total signal is considered an HFO. The custom code and parameters were then set to increasingly strict settings to reduce the amount of over detection while still detecting the HFO moments. This was done until the point where the false positives

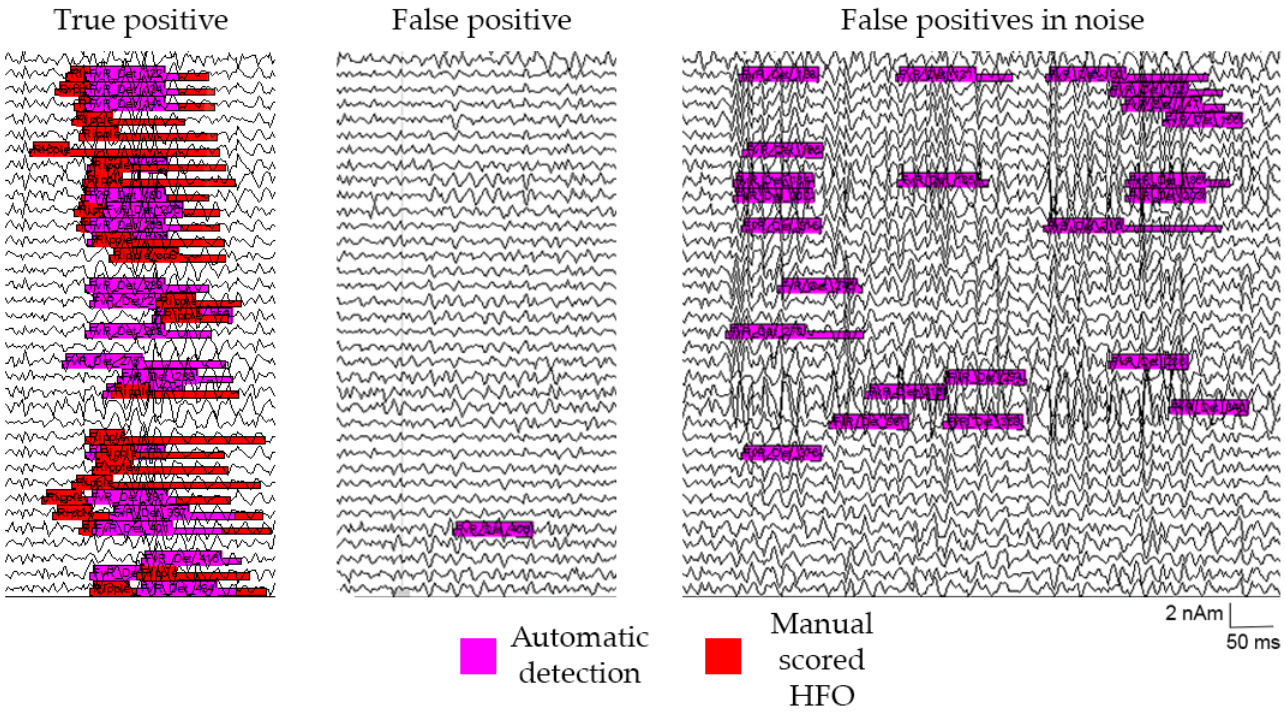

Figure 19: Example of a true positive, false positive and noise epoch. The left epoch shows automatic detections (shown in purple) at the same time as manual scored HFOs (shown in red) and is considered a true positive. The second epoch shows an automatic detection without co-occurring manual scored HFO, thus considered a false positive moment. The last epoch shows part of the signal with noise. The noise causes automatic detections, and these epochs were excluded from the analysis.

were reduced to a minimum and the HFOs spreading over multiple channels were still detected, at the cost of losing HFO moments with only a few (<3) detections. Automatic detections could then be classified in four categories: true positive when co-occurring with a marked HFO, false positive when not co-occurring with a marked HFO, false negative when an HFO moment was not detected and noise detection when the detection was caused by noise in the signal. The last category was introduced because noise was seen at continuous intervals and these intervals could subsequently be excluded from the analysis. The noise detection category makes it possible to exclude these detections from the performance calculations. Since some HFOs appear on more channels than others, the average number of manual scored HFOs was calculated for the false negative and true positive moments. The same was done for automatic detections in the false positive moments and noise epochs. This was done to give an indication of the number of erroneously detected HFOs. An example of a true positive, false positive and noise section is shown in figure 19. Since the goal was to detect the epileptogenic zone by using HFOs, it was decided to use settings where the majority of HFO times were correctly classified, with the least amount of false positive HFO times.

6.3 Results

The detector was run on the cxSSS pre-processed data of patient 9 before optimization and the addition of custom scripts described in section 4.2.1 to get a baseline score. This resulted in the detection of all 21 HFO times, but also in the detection of 86 false positive HFO times. 10 noise epochs where excluded from the analysis. The true positive HFO times show on average 12.4 detections, where the false positive HFO times show 2.77 detections on average. The excluded noise epochs contained on average 55.1 detections.

After optimization the detector was able to find 16 out of 21 HFO times. 13 false positive HFO times were detected and 9 noise detection epochs were present. The true positive HFO moments had an average of 11.2 channels where HFOs occurred. The average number of channels where HFOs occurred was 2.4 for the false negatives moments. The automatic detector made on average 2.6 erroneous detections per false positive

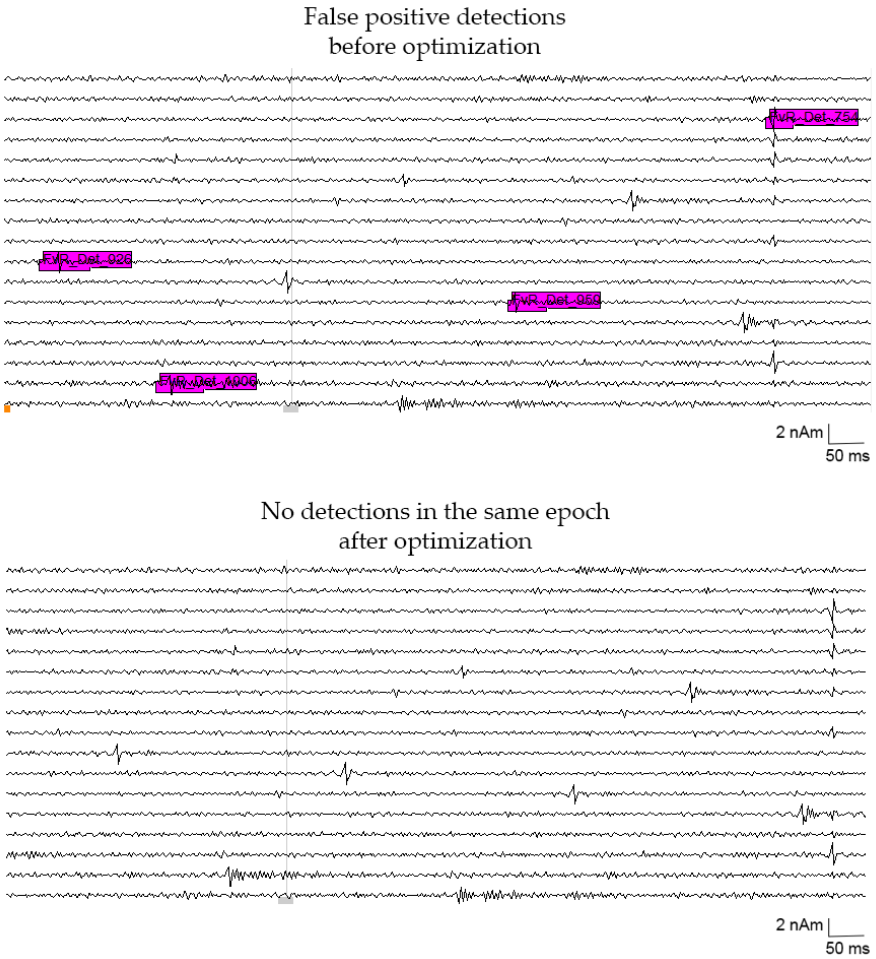

Figure 20: Example of the same two epochs of cxSSS pre-processed data using the all data beamformer. The top traces show the result of the detector before optimization. Three false positive moments are present. The bottom traces show the result of the detector after optimization, where the false positives of the top traces are not present anymore.

moment, and 27.9 erroneous detections per noise epoch. The optimized detector used a *BLmu* value of 0.85 and a *CDFlevel* value of 0.98.

An example of the difference in detection before and after optimization is presented in figure 20. This figure shows 4 false positives are present in the epoch when the detector is not optimized. The bottom graph shows the same epoch, after optimization of the detector. No more false positives are present.

6.4 Conclusion and discussion

The results of the optimization of the detector on cxSSS data shows that the majority of HFO times are detected after optimizing the detector. The HFO times that are not found show a smaller number of manual scored HFOs in comparison to the HFO times that are detected. This indicates that the automatic detector is able to find most HFO times where the HFOs are spread over multiple channels. Since the detector does not take neighboring channels into account, this can mean that the HFOs that spread over multiple channels are intrinsically different from HFOs that do not spread. Visual comparison of the different HFO moments shows that HFOs that are spread over multiple channels are larger in amplitude compared to HFO moments where the HFOs are not widely spread.

The optimized detector was not able to find all HFO moments. 16 out of 21 HFO times were detected, where the non-optimized detector found all HFO moments. The detection of all HFO moments was ac-

companied by a high number of false positives moments (86 in the non-optimized detector versus 13 in the optimized detector). Confidence that a detection is a true HFO is more important than the detection of all HFO moments at the cost of false positives, assuming the true HFOs originate from the same source.

Erroneous automatic detections are separated in two categories. The first is the noise detection category, where noise is detected as HFO. The average rate of 27.9 false detections per noise epoch is high, but the false detections caused by noise can easily be removed by excluding the noise epochs from the signal. The challenge lies in the false positive detections that occur outside the noise epochs. These are caused by the settings of the detector and the custom code. The detector shows a tradeoff between true positive HFO moments and false positive HFO moments. Full removal of the false positives was only possible at the cost of 9 true positive HFO moments, leaving 5 out of 21 true positive HFO times. In the results section it was shown that after optimization 13 false positive HFO moments were present with an average of 2.6 detections per channel. The reason to accept these settings for application to the total head volume is because the false positive HFO moments are well isolated from the true positive HFO moments and are only seen at a few channels on average. This should lead to a spatially isolated detection, not forming a cluster with other detections, and thus recognizable as noise.

Future versions of the detector should be able to use this clustering property of the beamformer, where HFOs are visible in multiple neighboring channels at the same time. After the detector has marked all HFOs in all channels, a subsequent step could be to check for every detection if there are simultaneous detections in (a certain percentage of) the neighboring channel, excluding false positive detections that are spatially separated. It should be noted that this method will not work in the ideal case, where the spatial resolution is high enough to only show HFOs in the VS where they originate.

The detector used for making the results is based on the Burnos detector [8]. This detector was created for the automatic detection of HFOs in intracranial EEG data. One of the main differences between HFOs measured with intracranial EEG and MEG is that HFOs deviate further from the baseline in intracranial EEG. The first step of the detector, the detection of EOIs, is based on this property. Since HFOs in MEG deviate less from the baseline, the results from this first detector step in MEG data are not as good when compared to results of the first detector step on intracranial data. Therefore another approach might be more suitable for the detection of HFOs in MEG. This approach should be based on the entropy of the signal. The current detector uses the entropy to compute the location of baseline segments but this process could be extended to the total signal. As explained earlier in this chapter, a low entropy value indicates a less 'random' and more oscillatory signal, and thus could be able to identify HFOs. Short experiments using the wavelet entropy [30] indicated that this method is currently too slow to use for the detection of HFOs in a large number of channels, but a future version might incorporate this technique for improved detection results in MEG.

7 Application of the beamformer and HFO detector on the total brain

7.1 Introduction

Chapter 5 showed how post-processing and applying a beamformer algorithm can increase the SNR and visualize HFOs in MEG data. Chapter 6 showed that it was possible to use a detector to localize most HFO moments in the processed MEG signal. In this chapter the beamformer was applied to create virtual sensors covering the whole brain and the automatic HFO detector was used to see if it was possible to localize the epileptogenic zone. This analysis was performed on the cxSSS dataset coming from patient 9.

7.2 Methods

To avoid missing HFOs in the brain, the whole brain volume has to be sampled by VSs. The locations where the beamformer algorithm calculates VSs were based on a list of x- y- z-coordinates. These coordinates were selected based on the co-registered MRI. A custom script was written to place VSs within the brain in a stacked checkerboard pattern. First the MRI was 'cut' under the nose, because the brain is located more superior to the level of the nose. The outline of the skull was determined using a custom script made by Arjan Hillebrand (VU Medical Center). To reduce the computational load of reconstructing one VS for every voxel, a grid of VSs was used. A square flat grid of VSs was placed on the lowest, most inferior, slice of the MRI, so at the level of the nose. VSs on the rows of the grid were spaced 6 mm apart from each other. The inter column distance was also 6 mm, and the rows were shifted 3 mm alternating between columns to create a checkerboard pattern. The next layer of VSs was placed 3 mm higher. The layer on this level was shifted 3 mm sideways, so VSs were not directly above each other and cover more area. The total height of the brain was filled like this, with alternating layers of VSs. All VSs located outside the head were removed. The x- y- z-coordinates of the remaining points were stored in a text file. An example of the locations for one layer of VSs in the brain is given in figure 21.

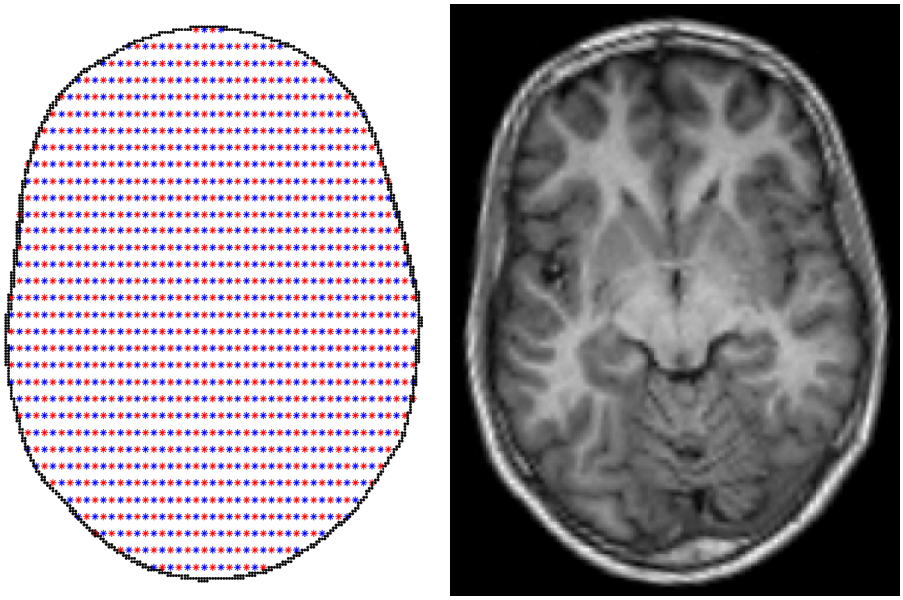

Figure 21: Example of two layers of VSs (left) based on the MRI-head shape (right). Every asterisk represents a single VS. Two layers of VSs are shown to illustrate the stacking checkerboard pattern. The red layer of VSs is placed 3 mm above the blue layer. The whole volume of the brain is filled with VSs using this pattern.

Another custom script was written to reconstruct all VS time traces at locations specified in the text file, and to save the resulting data on a hard disk. The original MEG recording consists of 306 channels. Based on these channels, around 24.000 VSs are constructed, leading to an 80 fold increase in file size compared to the original recording. The runtime to create all VSs was approximately 16 hours. After the reconstruction of all VSs was finished, the automated HFO detector ran on all VSs using the settings described in the previous

chapter, and the separate EOI and HFO detections were stored in one file each per VS. Each file contained the location of the VSs, starting time, peak frequency and duration for all detections in the specific VSs. The total runtime of the HFO detector was 54 hours.

To visualize the result of the detection, every x-y-slice where VSs were placed was plotted next to the corresponding MRI slice, and the number of detected HFOs was indicated by the color of the VSs. Since a retrospective dataset was used, the region with the highest number of HFOs could be compared to non-invasive data obtained in the pre-surgical workup and the area that was resected during surgery. Patient 9 underwent MRI, PET and SPECT imaging alongside MEG and EEG measurements. MRI findings showed a suspicion for mesotemporal sclerosis. Interictal EEG lateralized to the right, ictal EEG refined this to the right centro-temporal lobe. The PET scan showed activity in the temporo-parieto-occipital region, and the SPECT scan showed activity in the right temporo-pariatal region.

It was hypothesized that the total number of HFOs was higher on the affected side of the brain compared to the contralateral side, and that the epileptic focus could be found by looking at the clustering of the automatic detections.

7.3 Results

The first results presented are based on an analysis of the signal in all VSs and removing the detections occurring in 10 noise epochs. This resulted in many diffusely spread detections (figure 22). This figure shows the number of detections per VS using a color scale. The scale goes from no color when no HFOs were detected, to blue, which indicates a few detections, to purple, which indicates the most detections. The highest number of detections for a single VS was 9.

After plotting the results for the total time of the recording and excluding the noise epochs the separate HFO moments were analyzed. This meant plotting of all the detection results for all VSs at one specific moment. All separate HFO moments show the same spreading pattern, only the location of the false positives varies. This moment was chosen based on the manual HFO marks and the visual result of the detections. The result for one HFO moment is shown in the right column of figure 22. A red dot represents a VS where an HFO was detected. Apart from three detections in the cerebellum, the detections cluster to the right temporal lobe. A 3D plot showing the location of the detections for one HFO moment is shown in figure 23.

7.4 Conclusion and discussion

In this chapter the HFO detector was applied to VSs covering the total brain. Looking at all detections occurring during the length of the recording did not show a clear focus which is caused by the number of false positive detections. Most detections lateralized to the right side of the brain, but the midline, left temporal and left frontal lobe also showed detections. When the detections of one single HFO moment were plotted, the detections clustered in the right temporal lobe, although spread single detections were also present in the cerebellum.

It is possible to visually distinguish clusters from separate HFOs, and this makes it possible to determine the potential seizure onset zone. The information added by the detection of HFOs in MEG improved the delineation of the seizure onset zone. The MEG, used in the traditional way, could localize the potential epileptogenic zone to the right temporal side of the brain. Adding information about HFOs led to a more focal localization. The seizure onset zone matches well with the outcome of the pre-surgical evaluation. Both point to the right temporal lobe. ECoG and depth electrodes showed that the findings of the pre-surgical evaluation were the result of the spreading of the epileptiform activity from the small right occipital focus to the temporal and frontal regions as described in chapter 4. Based on this information it can be concluded that the automated detector indeed found channels with spread epileptiform activity in the form of HFOs, but that the small occipital focus was not found clearly. This might be caused by the size of the focus compared to the region of spreading.

The choice to use the MEG data of patient 9 for the detection of HFOs in the total head volume was based on the fact that there was a cleaned cxSSS version of the MEG recording for this patient. During the time

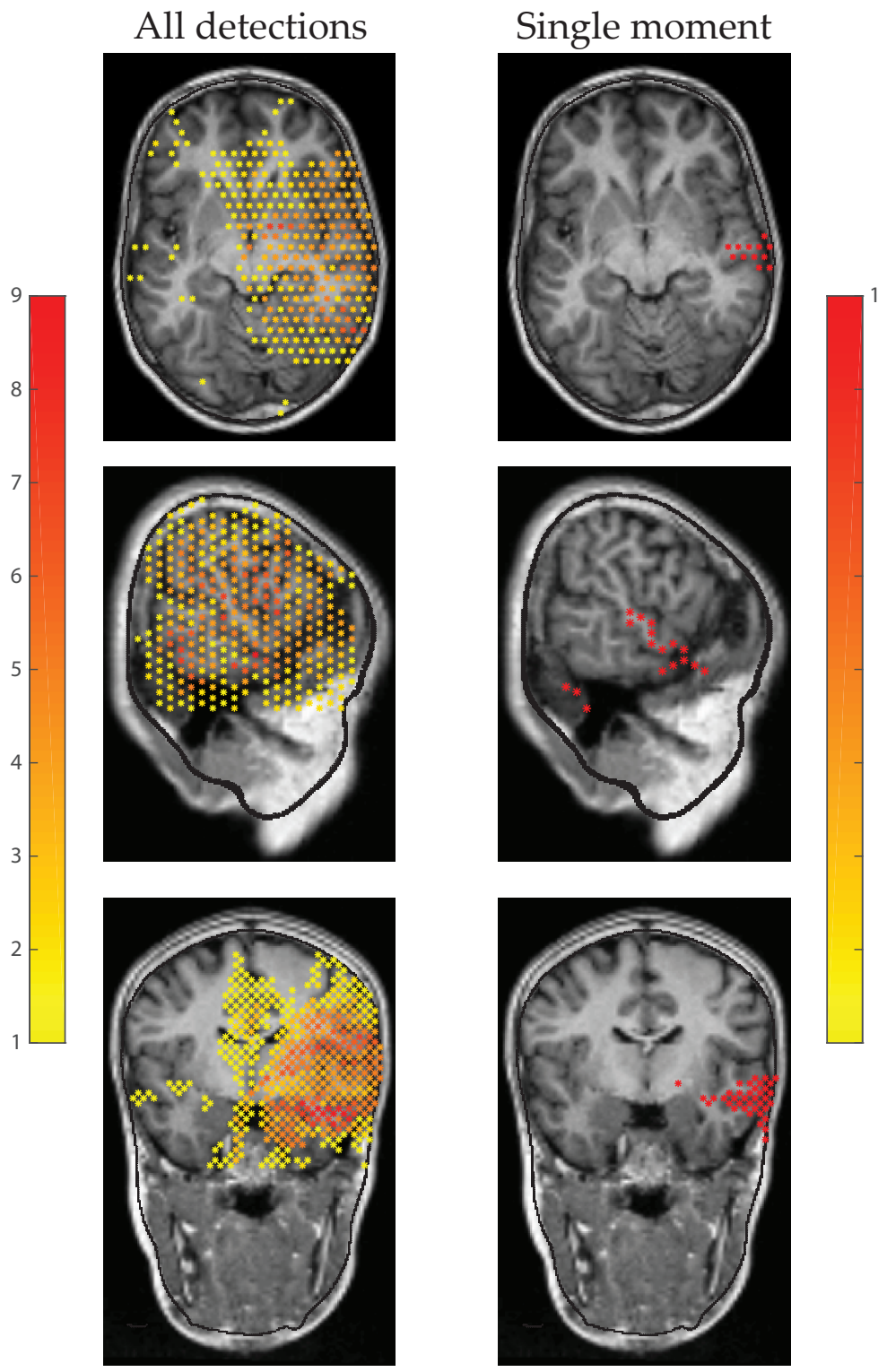

Figure 22: Example of the performance of the HFO detector on the total head showing two results. The left column shows the results when all detections during the total recording are considered, where the right column only considers the detections at a specific moment where it is known HFOs occur. The detections are shown as overlay on the corresponding MRI slice. A colored asterisk indicates an HFO is detected. In the left column, the color of the asterisk indicates the number of detections. Yellow indicates a low number of detections (1) and red indicates a high number of detections (9). In the right column a red asterisk represents a detection. The result of detections in the total recording are spread, mostly over the right hemisphere, and no clear focus is present. The results for the single HFO moment show a clustering in the right temporo-occipital region.

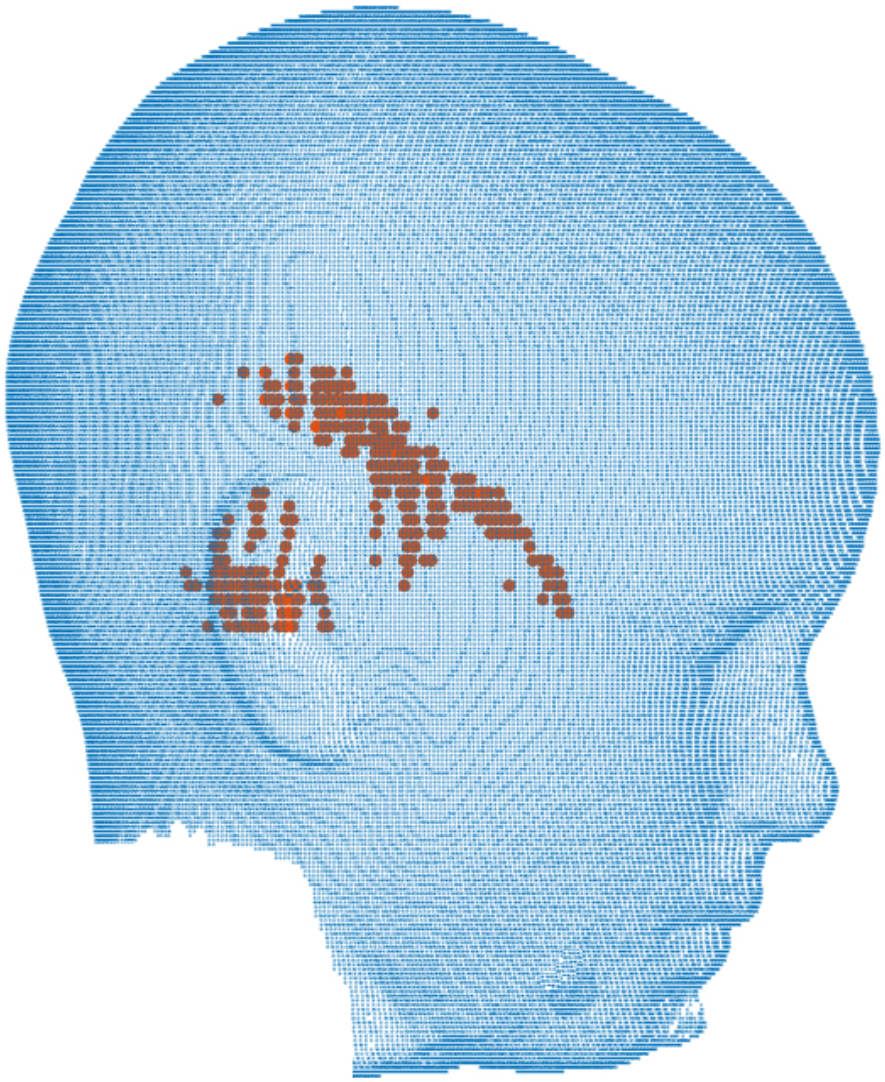

Figure 23: A three dimensional plot showing the results of the HFO detector when looking at one specific HFO moment. All detections are located in the right hemisphere.

of the analysis of the data, the information from the ECoG en depth electrodes revealed that patient 9 did not have an easy to determine epileptogenic zone. Future research should first focus on retrospective MEG data of patients with a clear epileptogenic focus, so a better comparison with non-invasive techniques can be performed.

8 General discussion

8.1 Principal findings

This study was the first to combine novel MEG techniques with an automatic HFO detector to localize the epileptogenic zone based on HFOs. It was possible to visualize HFOs in MEG using beamforming and to increase the SNR of the HFOs by using a combination of cxSSS pre-processing and beamformer settings. After optimization the detector was able to find the majority of HFO moments, and correctly lateralized the focus to be in the right hemisphere. More detailed spatial information was obtained by focusing on single HFO moments. This showed a clustering of the HFO detections in the right temporal lobe, in accordance with the pre-surgical evaluation. The combination of beamformer and HFO detector is able to run unsupervised, does not require visual scoring of epileptiform activity and can be performed on data acquired with the conventional clinical MEG protocol.

8.2 Relation to other studies

There is little literature on visual identified HFOs in MEG recordings. The first study showing HFOs in MEG in the time domain is very recent [40], and was the reason to start the study presented in this report. Earlier studies looking at high frequency MEG activity in time domain looked at evoked potentials [11]. Since evoked potentials are time locked they can be averaged to increase the SNR, a method not possible for spontaneous activity like HFOs. Other studies investigating spontaneous high frequency activity used methods based on time-frequency analysis [26, 28, 38, 49]. It is unclear how the results found by time-frequency analysis compare to the approach used in this report [20, 47, 51], since the time-frequency methods look at high frequency *activity* where the methods in this report are aimed at high frequency *oscillations*.

8.3 Strengths and weaknesess of the study

Application of the optimized HFO detector on VSs distributed over the total head localised the potential epileptogenic zone to the same region compared to other non-invasive techniques. Before the combination of techniques presented in this report can be applied in the clinic some issues have to be addressed. The results shown for the total head are made using data pre-processed with the new cxSSS algorithm. This algorithm is in the testing phase and as explained in chapter 5, there are currently some bugs in the software preventing clinical use. It was shown for one patient that pre-processed data improves the SNR of the HFOs, making the HFOs are easier to detect.

The best localization results were obtained using the manually scored HFOs to determine the true positive HFO moments. For clinical use it is not feasible to manually score HFOs for all patients. This can be solved by stepping through the signal only looking at moments where multiple detections occur at the same time in the same region, or by adding a step to the automatic detector to check if HFOs are not only detected in one single VS, but also in (a percentage of) neighboring VSs.

Generating the time traces and running the detector for all VSs is an automatic but time consuming process. The calculation time for one patient is approximately 3 days, although this process does not require supervision while running. One way to speed up this process is by a more strategic placement of VS. It is known from literature that the spatial resolution of the beamformer depends on the SNR of the pre-processed MEG signal, the depth, position and orientation of the reconstructed source and the head model used [4]. As a result of this, an HFO can be picked up by a VS at some distance from the original location. For this report a raster with equally spaced VSs was used with an inter-VS distance of 6 mm. Since the spatial resolution of the beamformer declines for deeper sources, it is not necessary to place VS close together in the deep structures since the region from where the VS will pick up signals overlaps. Van Klink *et al.* calculated a spatial resolution between 1 and 2 cm for the window beamformer using tSSS pre-processed data. Calculation of the spatial resolution of the all data beamformer using cxSSS should give an indication how close the VS should be placed next to each other. Another method to reduce the number of VS is by applying a gray matter mask. By using MRI segmentation techniques it is possible to create a mask showing only the location of the gray matter. Since HFOs are assumed to originate in the gray matter only, no VSs have to be placed in parts of the brain consisting of white matter. Removing unnecessary VSs yields a reduction in calculation time in

two ways. First the VS output does not have to be constructed, reducing the total time it takes to construct all VS (16 hours for the patient shown in this report), second the detector does not have to process the VS, reducing the total detection time (54 hours for the patient shown in this report). Another method to reduce the total calculation time is by parallel processing. The HFO detector can process VSs independent of each other, making it possible to process multiple VS in parallel. Currently only four VS could be processed at the same time, but when professional hardware with more parallel processing power is used the calculation time for the HFO detector can be greatly reduced (in fact the calculation time will be halved for every doubling of parallel processing units).

A fundamental challenge in MEG is finding deep sources. The SNR of MEG signals decreases towards the origin of the head. This might cause a problem for determining the epileptogenic zone in cases of hippocampal or other deep structures producing HFOs. On the other hand it is known that a decrease in SNR leads to a decrease in the spatial resolution of the beamformer, making the detection of a possible deep source less dependent on the correct placement of VSs.

The detector was optimized for the cxSSS data of patient 9. To use the detector in a clinical setting the settings of the detector should be self-learning or general for all patients. Currently some of the parameters are automatically scaling, but this scaling is largely dependent on how clean the part of the signal that is used to set the parameters is. Large artefacts may cause the detector to set parameters wrong and prevent the correct detection of HFOs.

Manual marked HFOs were used to verify the output of the detector. HFOs in MEG are not as clear as in intracranial EEG and it was shown for intracranial EEG that there is a large interrater variability when marking HFOs [51]. The HFOs were marked on the data used by van Klink *et al.*, which used the window beamformer for pre-processing. This means that some HFOs might have changed in appearance for the different beamformer algorithms, or disappeared because of a change in beamformer spatial resolution caused by a difference in SNR between pre-processing techniques. This can affect the number of true and false positives reported in this study.

The retrospective dataset used for this thesis contains MEG data sampled at 1250 Hz, with a 410 Hz anti-aliasing filter applied. Because it was not possible to measure the full fast ripple band (250-500 Hz) and because the head localization coils influence the signal around 300 Hz, it was chosen to focus on the detection of ripples (80-250 Hz). It is known from literature that fast ripples are a better biomarker for the epileptogenic zone compared to ripples [41]. The new version of the MEG software that is announced contains, apart from the cxSSS algorithm, also a function to remove the head coil signals from the recording, making it possible to look at fast ripples and possibly improving the result of the localization of the EZ.

Due to technical aspects explained in chapter 5 the results in the final chapters of this report are based on one patient. It was chosen to analyze this one patient instead of 8 other patients, because the SNR of the cxSSS file, available for this patient, was significantly higher compared to the tSSS files of the same patient. Since the SNR has a big influence on the performance of the beamformer and because it is expected that the cxSSS algorithm will be available in the near future, it was decided to show what is possible with this new pre-processing algorithm in combination with optimal beamformer settings.

8.4 Clinical relevance of the study

Obtaining an accurate hypothesis on the location of the epileptogenic zone using HFOs in MEG is a step towards improvement of the non-invasive detection of the epileptogenic zone. Using information about HFOs, it was possible to narrow down the hypothesis on the location of the epileptogenic zone to the right temporal lobe. This report showed that it is possible to detect HFOs with an automated workflow where only little human input was needed, although invasive techniques showed that the found HFOs were not the source, but spread from a small occipital focus. The method is not depending on a human reviewer, in comparison to traditional HFO research and the MEG has a potential good spatial resolution. If the techniques presented in this report are more refined, more patients can be send for MEG investigation. This can be seen as a firm step towards a non-invasive, user independent technique that can be used to assist in the planning of epilepsy surgery.

8.5 Future research

This thesis investigated the practical possibilities of automatic non-invasive HFO detection in MEG recordings. It was shown that using new pre-processing techniques and beamformer analysis it is possible to find HFOs in the brain and to produce a hypothesis for the location of the EZ.

The current work shows the results of the HFO detection in the total brain volume for one patient. As soon as the new version of the MEG software is released, the same analysis can be performed on the remaining 7 patients. This will allow for the comparison of the cxSSS pre-processed data in combination with the all data beamformer and the tSSS pre-processed data in combination with the all data beamformer. It will also allow to draw a more solid conclusion on the localization result of the detected HFOs.

In future work more information about detected HFOs can be used. The detector used in this thesis is able to give information about the duration and frequency of detected HFOs. This can be used to investigate whether there is a correlation between HFO length and the EZ or the frequency of the HFO and the EZ. Especially the HFO frequency has been shown to play a role in the localization of the EZ, where higher frequencies tend to be more specific compared to lower frequencies [41]. Due to the low sampling rate and interference of the head localizatin coils this thesis focused at ripples. A new study has already started, recording resting state MEG in epilepsy patients with a sample frequency of 2000 Hz, enabling the investigation of both ripples and fast ripples in the near future.

In this thesis HFOs were used to form a hypothesis on the location of the EZ. Another method to use HFOs could be to monitor the effect of AEDs in epilepsy patients. It was shown that the rate of HFOs mirrors disease activity in patients [53, 22]. Using this information it should be possible to tailor medication to the need of individual patients and to prevent or reduce the side effects of AEDs.

The future goal for the technique presented in this thesis is not to add a new measuring method to the list of already existing non-invasive imaging and electrographic measuring techniques, but to replace them. Ideally three modalities are needed for the planning of surgery. First there is need for imaging of the brain, to detect structural anomalies. This can be done by using MRI, as is already standard practice. The second modality should present insight in the electrophysiology of the brain. This is where MEG should be used, based on the ability to detect HFOs and the high spatial resolution compared to other non-invasive modalities [23]. The brain can be scanned for the currently considered best electrophysiological biomarker, HFOs, using the reviewer independent analysis presented in this thesis. This information, combined with the information from the MRI, should indicate where the EZ is most likely located. Intra-operative methods such as ECoG can then be applied to fine tune the resection of the epileptogenic tissue.

References

[1] Adjamian, P., Worthen, S. F., Hillebrand, A., Furlong, P. L., Chizh, B. A., Hobson, A. R., Aziz, Q., and Barnes, G. R. (2009). Effective electromagnetic noise cancellation with beamformers and synthetic gradiometry in shielded and partly shielded environments. *Journal of Neuroscience Methods*, 178(1):120–127.

[2] Alarcon, G. (1997). Origin and propagation of interictal discharges in the acute electrocorticogram. Implications for pathophysiology and surgical treatment of temporal lobe epilepsy. *Brain*, 120(12):2259–2282.

[3] Andrade-Valenca, L. P., Dubeau, F., Mari, F., Zelmann, R., and Gotman, J. (2011). Interictal scalp fast oscillations as a marker of the seizure onset zone. *Neurology*, 77(6):524–531.

[4] Barnes, G. R., Hillebrand, A., Fawcett, I. P., and Singh, K. D. (2004). Realistic spatial sampling for MEG beamformer images. *Human brain mapping*, 23(2):120–7.

[5] Bragin, A., Engel, J., Wilson, C. L., Fried, I., and Buzsáki, G. (1999a). High-frequency oscillations in human brain. *Hippocampus*, 9(2):137–142.

[6] Bragin, A., Engel, J., Wilson, C. L., Fried, I., and Mathern, G. W. (1999b). Hippocampal and entorhinal cortex high-frequency oscillations (100-500 Hz) in human epileptic brain and in kainic acid-treated rats with chronic seizures. *Epilepsia*, 40(2):127–137.

[7] Brookes, M. J., Vrba, J., Robinson, S. E., Stevenson, C. M., Peters, A. M., Barnes, G. R., Hillebrand, A., and Morris, P. G. (2008). Optimising experimental design for MEG beamformer imaging. *NeuroImage*, 39(4):1788–802.

[8] Burnos, S., Hilfiker, P., Sürücü, O., Scholkmann, F., Krayenbühl, N., Grunwald, T., and Sarnthein, J. (2014). Human intracranial high frequency oscillations (HFOs) detected by automatic time-frequency analysis. *PloS one*, 9(4):e94381.

[9] Chang, B. S. and Lowenstein, D. H. (2003). Epilepsy. *New England Journal of Medicine*, 349(13):1257–1266.

[10] Crépon, B., Navarro, V., Hasboun, D., Clemenceau, S., Martinerie, J., Baulac, M., Adam, C., and Le Van Quyen, M. (2010). Mapping interictal oscillations greater than 200 Hz recorded with intracranial macroelectrodes in human epilepsy. *Brain*, 133(1):33–45.

[11] Curio, G., Mackert, B. M., Burghoff, M., Koetitz, R., Abraham-Fuchs, K., and Härer, W. (1994). Localization of evoked neuromagnetic 600 Hz activity in the cerebral somatosensory system. *Electroencephalography and clinical neurophysiology*, 91(6):483–7.

[12] Foffani, G., Uzcategui, Y. G., Gal, B., and Menendez de la Prida, L. (2007). Reduced Spike-Timing Reliability Correlates with the Emergence of Fast Ripples in the Rat Epileptic Hippocampus. *Neuron*, 55(6):930–941.

[13] Forsgren, L., Beghi, E., Õun, A., and Sillanpää, M. (2005). The epidemiology of epilepsy in Europe - A systematic review. *European Journal of Neurology*, 12(4):245–253.

[14] Hansen, P., Kringelbach, M., and Salmelin, R. (2010). *MEG: An introduction to methods*. Oxford University Press.

[15] Harroud, A., Bouthillier, A., Weil, A. G., and Nguyen, D. K. (2012). Temporal Lobe Epilepsy Surgery Failures: A Review. *Epilepsy Research and Treatment*, 2012:1–10.

[16] Hillebrand, A. and Barnes, G. R. (2003). The use of anatomical constraints with MEG beamformers. *NeuroImage*, 20(4):2302–13.

[17] Hillebrand, A. and Barnes, G. R. (2005). Beamformer analysis of MEG data. *International review of neurobiology*, 68(05):149–71.

[18] Holsheimer, J. and Feenstra, B. (1977). Volume conduction and eeg measurements within the brain: A quantitative approach to the influence of electrical spread on the linear relationship of activity measured at different locations. *Electroencephalography and clinical neurophysiology*, 43:52–58.

[19] Jacobs, J., Levan, P., Chtillon, C. D., Olivier, A., Dubeau, F., and Gotman, J. (2009). High frequency oscillations in intracranial EEGs mark epileptogenicity rather than lesion type. *Brain*, 132(4):1022–1037.

[20] Jacobs, J., Staba, R., Asano, E., Otsubo, H., Wu, J. Y., Zijlmans, M., Mohamed, I., Kahane, P., Dubeau, F., Navarro, V., and Gotman, J. (2012). High-frequency oscillations (HFOs) in clinical epilepsy. *Progress in neurobiology*, 98(3):302–15.

[21] Jefferys, J. G. R., Menendez de la Prida, L., Wendling, F., Bragin, A., Avoli, M., Timofeev, I., and Lopes da Silva, F. H. (2012). Mechanisms of physiological and epileptic HFO generation. *Progress in neurobiology*, 98(3):250–64.

[22] Kobayashi, K., Akiyama, T., Oka, M., Endoh, F., and Yoshinaga, H. (2015). A storm of fast (40-150Hz) oscillations during hypsarrhythmia in West syndrome. *Annals of neurology*, 77(1):58–67.

[23] Lu, Y., Worrell, G. A., Zhang, H. C., Yang, L., Brinkmann, B., Nelson, C., and He, B. (2014). Noninvasive imaging of the high frequency brain activity in focal epilepsy patients. *IEEE transactions on bio-medical engineering*, 61(6):1660–7.

[24] Lüders, H. O., Najm, I., Nair, D., and Widdess-Walsh, P. (2006). The epileptogenic zone : general principles. *Epileptic Disorders*, 8(Suppl. 2):1–9.

[25] Melani, F., Zelmann, R., Dubeau, F., and Gotman, J. (2013). Occurrence of scalp-fast oscillations among patients with different spiking rate and their role as epileptogenicity marker. *Epilepsy Research*, 106(3):345–356.

[26] Miao, A., Xiang, J., Tang, L., Ge, H., Liu, H., Wu, T., Chen, Q., Hu, Z., Lu, X., and Wang, X. (2014). Using ictal high-frequency oscillations (80-500Hz) to localize seizure onset zones in childhood absence epilepsy: a MEG study. *Neuroscience letters*, 566:21–6.

[27] Papadelis, C., Poghosyan, V., Fenwick, P. B. C., and Ioannides, A. A. (2009). MEG's ability to localise accurately weak transient neural sources. *Clinical Neurophysiology*, 120(11):1958–1970.

[28] Rampp, S., Kaltenhäuser, M., Weigel, D., Buchfelder, M., Blümcke, I., Dörfler, A., and Stefan, H. (2010). MEG correlates of epileptic high gamma oscillations in invasive EEG. *Epilepsia*, 51(8):1638–1642.

[29] Rosenow, F. and Lu, H. (2001). Presurgical evaluation of epilepsy. *Brain*, pages 1683–1700.

[30] Rosso, O. A., Blanco, S., Yordanova, J., Kolev, V., Figliola, A., Schurmann, M., and Basar, E. (2001). Wavelet entropy: a new tool for analysis of short duration brain electrical signals. *Journal of neuroscience methods*, 105(1):65–75.

[31] Siegel, A. M. (2004). Presurgical evaluation and surgical treatment of medically refractory epilepsy. *Neurosurgical review*, 27(1):1–18; discussion 19–21.

[32] Staba, R. J., Wilson, C. L., Bragin, A., Fried, I., and Engel, J. (2002). Quantitative analysis of high-frequency oscillations (80-500 Hz) recorded in human epileptic hippocampus and entorhinal cortex. *Journal of neurophysiology*, 88(4):1743–1752.

[33] Stockwell, R. G., Mansinha, L., and Lowe, R. P. (1996). Localization of the complex spectrum: The S transform. *IEEE Transactions on Signal Processing*, 44(4):998–1001.

[34] Taulu, S. and Hari, R. (2009). Removal of magnetoencephalographic artifacts with temporal signal-space separation: Demonstration with single-trial auditory-evoked responses. *Human Brain Mapping*, 30(5):1524–1534.

[35] Taulu, S., Kajola, M., and Simola, J. (2004). Suppression of interference and artifacts by the signal space separation method. *Brain Topography*, 16(4):269–275.

[36] Taulu, S. and Simola, J. (2006). Spatiotemporal signal space separation method for rejecting nearby interference in MEG measurements. *Physics in medicine and biology*, 51(7):1759–1768.

[37] Tellez-Zenteno, J. F., Dhar, R., and Wiebe, S. (2005). Long-term seizure outcomes following epilepsy surgery: a systematic review and meta-analysis. *Brain*, 128(5):1188–1198.

[38] Tenney, J. R., Fujiwara, H., Horn, P. S., Vannest, J., Xiang, J., Glauser, T. A., and Rose, D. F. (2014). Low- and high-frequency oscillations reveal distinct absence seizure networks. *Annals of neurology*, 76(4):558–67.

[39] van Klink, N., Frauscher, B., Zijlmans, M., and Gotman, J. (2015a). Relationships between interictal epileptic spikes and ripples in surface EEG. *Clinical Neurophysiology*.

[40] van Klink, N., Hillebrand, A., and Zijlmans, M. (2015b). Identification of epileptic high frequency oscillations in the time domain by using MEG beamformer-based virtual sensors. *Clinical neurophysiology*.

[41] van 't Klooster, M. A., van Klink, N. E. C., Leijten, F. S. S., Zelmann, R., Gebbink, T. A., Gosselaar, P. H., Braun, K. P. J., Huiskamp, G. J. M., and Zijlmans, M. (2015). Residual fast ripples in the intraoperative corticogram predict epilepsy surgery outcome. *Neurology*.

[42] von Ellenrieder, N., Andrade-Valença, L. P., Dubeau, F., and Gotman, J. (2012). Automatic detection of fast oscillations (40–200Hz) in scalp EEG recordings. *Clinical Neurophysiology*, 123(4):670–680.

[43] Vrba, J. (2002). Magnetoencephalography: the art of finding a needle in a haystack. *Physica C*, 25:1–9.

[44] Vrba, J. and Robinson, S. E. (2001). Signal processing in magnetoencephalography. *Methods*, 25(2):249–271.

[45] Wiebe, S., Blume, W. T., Girvin, J. P., and Eliasziw, M. (2001). A Randomized, Controlled Trial of Surgery for Temporal-Lobe Epilepsy. *New England Journal of Medicine*, 345(5):311–318.

[46] Worrell, G. and Gotman, J. (2011). High-frequency oscillations and other electrophysiological biomarkers of epilepsy: clinical studies. *Biomarkers in medicine*, 5(5):557–66.

[47] Worrell, G. A., Jerbi, K., and Kobayashi, K. (2012). Recording and analysis techniques for high-frequency oscillations. *Progress in Neurobiology*, 98(3):265–278.

[48] Wu, J. Y., Koh, S., Sankar, R., and Mathern, G. W. (2008). Paroxysmal fast activity: an interictal scalp EEG marker of epileptogenesis in children. *Epilepsy research*, 82(1):99–106.

[49] Xiang, J., Liu, Y., and Wang, Y. (2009). Frequency and spatial characteristics of high-frequency neuromagnetic signals in childhood epilepsy. *Epileptic disorders*, 11(2):113–125.

[50] Zelmann, R., Mari, F., Jacobs, J., Zijlmans, M., Chander, R., and Gotman, J. (2010). Automatic detector of High Frequency Oscillations for human recordings with macroelectrodes. In *2010 Annual International Conference of the IEEE Engineering in Medicine and Biology*.

[51] Zelmann, R., Zijlmans, M., Jacobs, J., Châtillon, C.-E., and Gotman, J. (2009). Improving the identification of High Frequency Oscillations. *Clinical neurophysiology*, 120(8):1457–64.

[52] Zijlmans, M., Jacobs, J., Kahn, Y. U., Zelmann, R., Dubeau, F., and Gotman, J. (2011). Ictal and interictal high frequency oscillations in patients with focal epilepsy. *Clinical Neurophysiology*, 122(4):664–671.

[53] Zijlmans, M., Jacobs, J., Zelmann, R., Dubeau, F., and Gotman, J. (2009). High-frequency oscillations mirror disease activity in patients with epilepsy. *Neurology*, 72(11):979–86.

[54] Zijlmans, M., Jiruska, P., Zelmann, R., Leijten, F. S. S., Jefferys, J. G. R., and Gotman, J. (2012). High-frequency oscillations as a new biomarker in epilepsy. *Annals of neurology*, 71(2):169–78.

9 Appendix

A Abstract for the 31st International Epilepsy Congress in Istanbul

Automatic identification of the epileptogenic zone based on High Frequency Oscillations in MEG

Frank van Rosmalen[a,b], Nicole van Klink[a], Maeike Zijlmans[a,c], Arjan Hillebrand[d]

[a] Brain Center Rudolf Magnus, Department of Neurology and Neurosurgery, University Medical Center Utrecht The Netherlands.
[b] MIRA Institute for Biomedical Technology and Technical Medicine, Twente University, Enschede, The Netherlands.
[c] SEIN – Stiching Epilepsie Instellingen Nederland, Heemstede, The Netherlands
[d] Department of Clinical Neurophysiology and Magnetoencephalograpy Center, VU University Medical Center, Amsterdam, The Netherlands

Purpose: High frequency oscillations (HFOs, >80Hz) are a biomarker for the epileptogenic zone (EZ). Our final goal is to automatically localize the HFO region using magnetoencephalography (MEG).

Methods: Fifteen minutes of resting state MEG data were selected in 12 patients. We increased the signal to noise ratio in MEG recordings by computing spatial filters using beamforming, and used this technique to reconstruct time series (virtual sensors, VS) for a priori defined brain regions. As a first step we placed VS around the epileptic spikes (affected region) and in the contralateral hemisphere. We manually marked HFOs and spikes in MEG in the time domain in these VS. The time points with HFOs in VS were reviewed in the physical sensors. The next step will be to use a detector to automatically identify HFOs for all brain regions (a task which is too time-consuming to do manually) and to generate a 3D map to reveal regions with HFOs.

Results: We identified 575 HFOs in VS, at 78 points in time, in eight patients. 513 HFOs were in the affected region. HFOs could not be visually identified in physical sensors for 61 of the 78 time points that showed HFOs in VS. These manually marked HFOs will be used to optimize an automatic detection algorithm.

Conclusion: Beamformer-based VS analysis can help to identify HFOs that are not discernable in physical MEG sensors. This step eases the automatic detection of the HFO region. These findings are a preliminary step towards our goal: to automatically localize the HFO region in patients with focal epilepsy using MEG. This map can be used to tailor epilepsy surgery.

Automatic identification of the epileptogenic zone based on high frequency oscillations in MEG

VUmc UNIVERSITY OF TWENTE. Brain Center Rudolf Magnus

F. van Rosmalen[1,2], N. van Klink[1], M. Zijlmans[1,3], A. Hillebrand [4]

1) University Medical Center Utrecht, Department of Neurology and Neurosurgery, Utrecht, The Netherlands 2) MIRA Institute for Biomedical Technology and Technical Medicine, Enschede, The Netherlands 3) SEIN – Stichting Epilepsie Instellingen Nederland, Heemstede, The Netherlands 4) VU University Medical Center, Department of Clinical Neurophysiology and Magnetoencephalography Center, Amsterdam, The Netherlands

Purpose

High frequency oscillations (HFOs, >80Hz) are a biomarker for the epileptogenic zone (EZ). Automatic non-invasive identification of the EZ by detection of HFOs in **MEG** could help in the surgical planning of epilepsy surgery.

Aim

To develop a method for the **automatic identification** of the epileptogenic zone based on **HFOs** in MEG.

Method

Data aquisition:

- 2 patients with retractable epilepsy.
- 15 mins of resting state MEG.

Processing:

- Remove MEG sensor noise and artifacts
- Use **beamformer** algorithm to increase signal-to-noise ratio (SNR)
- Reconstruct local time series ('virtual sensors', VS) for ~25.000 locations in the brain.
- Use an adapted version of the Burnos **HFO-detector** [1] to automatically mark HFOs in VS.

Analysis:

- Check if the **number of detected HFOs** per VS indicate a clear EZ.
- Compare the detected EZ with the resected area.

Results

Signal-to-Noise Ratio (SNR)

Raw MEG data:

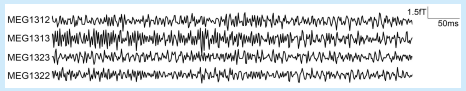

Pre-processed MEG data:

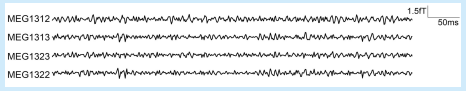

Beamformer virtual sensor result:

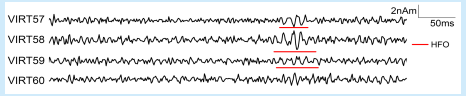

Fig 1. 80Hz high pass filtered MEG sensor data from one patient. No HFOs are visible. A) Raw MEG data. B) Preprocessed MEG data. C) 80Hz high pass filtered beamformer VS around the same location and at the same time as A and B, HFOs are visible.

HFO Detection in MEG

Example for a subset of 70 virtual sensors of one patient (Fig. 4A)

- 14/21 moments where HFOs occur were automatically identified
- 160 identified moments where HFOs occur were false positive

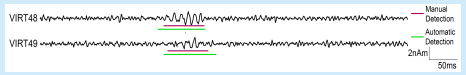

Fig 2. Examples of true positive marked HFOs.

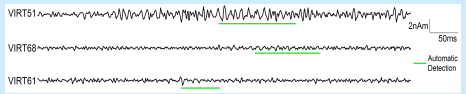

Fig 3. Examples of false positive marked HFOs.

Identification of the epileptogenic zone

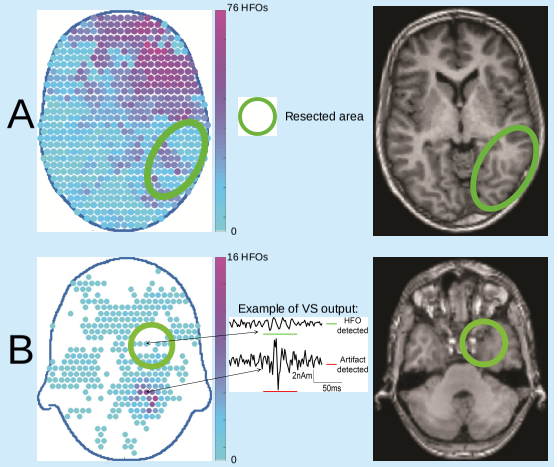

Fig 4. Results of automatic HFO detection compared with the resected area (green circle) for both patients. One colored dot represents one VS. A) The majority of detections are in the right frontal region, resected area: right temporo-occipital. B) The majority of detections are in the cerebellum, resected area: right amygdala/hippocampus.

Conclusion:

- It is possible to automatically find HFOs using MEG.
- We have successfully constructed local time series for the total brain
- Unfortunately the clinical EZ is not yet detected due to false positives found by the automatic detector.

Discussion:

- Visual inspection showed most false positives are caused by signal artifacts. More work is needed to show if the identification of the EZ improves when the artifacts are removed.

[1] Burnos S, Hilfiker P, Sürücü O, Scholkmann F, Krayenbühl N, Grunwald T, et al. (2014) Human Intracranial High Frequency Oscillations (HFOs) Detected by Automatic Time-Frequency Analysis. PLoS ONE 9(4): e94381.

University Medical Center Utrecht

Contact: f.vanrosmalen@student.utwente.nl